

# Cell-Free Massive MIMO for Wireless Federated Learning

Tung T. Vu, Duy T. Ngo, Nguyen H. Tran, Hien Quoc Ngo, Minh N. Dao, and Richard H. Middleton

**Abstract**—This paper proposes using cell-free massive multiple-input multiple-output (MIMO) systems to support federated learning (FL) in wireless networks. Thanks to their channel hardening property, these systems provide stable channel conditions for the FL processes to operate on. With a high probability of coverage, they also make the FL processes less prone to the users with unfavorable links. Here, we formulate an FL training time minimization problem where the local accuracy, transmit power, data rate, and users' processing frequency are jointly optimized. This mixed-timescale stochastic nonconvex problem captures the complex interactions among the training time, and transmission and computation of training updates of one FL process. By employing the online successive convex approximation approach, we develop a new algorithm to solve the formulated problem with proven convergence to the neighbourhood of its stationary points. The proposed algorithm only requires channel stability in each iteration rather than its entire run time. Our numerical results confirm that the presented joint design reduces the training time by up to 55% over baseline approaches. They also show that cell-free massive MIMO here requires the lowest training time for FL processes compared with cell-free time-division multiple access massive MIMO and collocated massive MIMO.

**Index Terms**—Cell-free massive MIMO, federated learning.

## I. INTRODUCTION

The use of machine learning (ML) techniques in telecommunications industry has been growing dramatically in recent years [1]–[4]. One reason for this trend is the fast growing number of mobile devices, wearable devices and autonomous vehicles. They are generating a vast amount of data by using in-built sensors, e.g., microphones, GPS and camera, for critical applications such as traffic navigation, indoor localization, image recognition, natural language processing, and augmented reality [5]–[7]. In addition, the computational capabilities of these devices also grow significantly with dedicated hardware architecture and computing engines, e.g., the energy-efficient Qualcomm Hexagon Vector eXtensions on Snapdragon 835 [8]. On-device artificial intelligence (AI) capabilities are predicted to be available on 80% of all smartphones by 2022 [9]. It is therefore critical for telecommunications operators to start investigating into a future communications

T. T. Vu, D. T. Ngo and R. H. Middleton are with the School of Electrical Engineering and Computing, The University of Newcastle, Callaghan, NSW 2308, Australia (e-mail: thanhtung.vu@uon.edu.au; {duy.ngo, richard.middleton}@newcastle.edu.au).

N. H. Tran is with the School of Computer Science, The University of Sydney, Sydney, NSW 2006, Australia (e-mail: nguyen.tran@sydney.edu.au).

H. Q. Ngo is with the School of Electronics, Electrical Engineering and Computer Science, Queen's University Belfast, Belfast BT7 1NN, United Kingdom (e-mail: hien.ngo@qub.ac.uk).

M. N. Dao is with the Priority Research Centre for Computer-Assisted Research Mathematics and its Applications (CARMA), The University of Newcastle, Callaghan, NSW 2308, Australia (e-mail: daonminh@gmail.com).

system that efficiently utilizes the empowered computation resources from mobile devices to solve ML problems.

The typical ML framework used in the current telecommunications systems requires a cloud center to store and process raw data collected by the user equipment (UEs). However, such a centralized structure fails to support real-time applications because of its high latency [10]. The concept of mobile edge computing is introduced to process data at the edge nodes instead of the cloud center [11]–[13]. Since the computational capability of mobile devices is growing noticeably, it is possible to even push the network computation further to the mobile device level. On the other hand, serious concerns about data privacy have recently been raised due to data being processed by third-party companies, e.g., Facebook, Apple. This urgently calls for a new class of ML frameworks that not only exploit the computational resources of the UEs for ML applications but also ensure data privacy.

A promising candidate for such ML frameworks is the recently developed Federated Learning (FL) [14]–[17]. In this framework, an FL process can be considered as an iterative process in which the UEs use their local training data to compute local model training updates, followed by sending the updates to a central server. The central server then aggregates these updates to compute the global training update, which is then sent back to the UEs to further assist their local update computation. This iterative process terminates when a certain learning accuracy level is attained. Data privacy is protected by not sharing the local training *data*, but only the local *training updates* computed at the UEs using local computational resources. Uploading only the local training updates to the central server incurs a significantly lower delay, compared to uploading a large amount of raw data. This distributed approach facilitates a large-scale model training and more flexible data collection, albeit at the expense of UEs' computational resources [18].

With all the promising advantages listed above, FL has attracted much attention from both developer and researcher communities [18]–[26]. In [19], an FL algorithm for keyboard prediction on smartphones is developed by Google. [20] builds a scalable production system for FL in real mobile devices using TensorFlow. [21] and [22] target improving the performance of the general FL algorithms, while [18], [23]–[27] concentrate on optimizing the performance of FL algorithms used in wireless networks. In particular, [21] proposes a new compression framework for a communication-efficient FL system. The statistical heterogeneity issues of UEs are addressed in [22]. [18] aims to obtain the best trade-off between FL training time and UE energy consumption. [23] proposes an

incentive mechanism that encourages the UEs with high-quality data to participate in FL systems. [24] introduces a control algorithm to achieve the best trade-off between the number of local updates and that of global updates for a given resource budget. A joint device selection and beamforming design is proposed in [25] to enhance the performance of FL. [26] proposes a bandwidth allocation and scheduling scheme that reduces the network energy consumption while guaranteeing performance for FL. [27] proposes a joint design of user selection, power control and subchannel allocation for minimizing the loss function of FL.

This paper investigates how to implement FL in a wireless network. It is worth noting that the existing works [18], [25] rely on an impractical assumption that the channel state information (CSI) remains unchanged during the whole FL process. In practice however, the channel changes in the order of milliseconds; and as such, certain system parameters for FL performance optimization, e.g., data rates and power control, would have become obsolete even before the FL process terminates. In addition, it might not be most efficient to use orthogonal multiplexing approaches, e.g., orthogonal frequency-division multiple access (OFDMA) [26], [27] and time-division multiple access (TDMA) [18], for UEs to transmit their local updates. With a large number of UEs, the total training time could be significantly prolonged. To both deal with the wireless channel dynamics and to serve UEs at the same time and in the same frequency bands, a new wireless network structure that supports FL is called for.

In this work, we propose using cell-free massive multiple-input multiple-output (MIMO) [28]–[31] for FL in a wireless environment. Here, a central processing unit (CPU) (i.e., the central server) is connected to a large number of access point (APs) via backhaul links. These APs then simultaneously serve UEs via wireless links using the same frequency bands with the CSI acquired via uplink (UL) training pilots. An important characteristic of massive MIMO is channel hardening [32], i.e., the effective channel gain at the UEs is close to its expected value—a known deterministic constant [31]. As the channel is stable during one large-scale coherence time  $\tilde{T}_c$ <sup>1</sup>, the channel dynamics due to small-scale fading have negligible effects on the FL processes. In addition, a cell-free massive MIMO network also provides a high probability of coverage, making the FL processes less prone to the unfavorable UE links.

Our research contributions are summarized as follows.

- We propose, for the first time, a general scheme for cell-free massive MIMO networks to support FL. In this scheme, any iterative algorithm can be developed to optimize the FL performance before the FL process is executed. Each instead of all iterations of this FL optimization algorithm or the FL process is required to happen within one  $\tilde{T}_c$  in order to guarantee channel stability during its operation. In each iteration of the FL process, we propose using the APs as relays to transmit

<sup>1</sup>During one large-scale coherence time  $\tilde{T}_c$ , the large-scale fading coefficients are reasonably invariant. The value of  $\tilde{T}_c$  can be empirically measured, in the same way for small-scale fading measurement. For indoor communications, the large-scale coherence time can be at least 40 small-scale fading coherence time [31], and it has a time order of seconds.

the training updates between the CPU and UEs. Doing so allows any beamforming/filtering design to be applied to the APs in order to enhance the performance of training update transmission.

- Targeting the key performance metric of “training time minimization”, we formulate a mixed-timescale stochastic nonconvex optimization problem that minimizes the time of one FL process. The formulated problem captures the complex interactions among the FL training time, and transmission and computation of FL training updates in a cell-free massive MIMO network. Here, a conjugate beamforming/matched filtering scheme is applied to the APs for ease of implementation. The local accuracy, power control, data rate and UE’s processing frequency are jointly designed, subject to the practical constraints on UEs’ energy consumption and imperfect channel estimation.
- Utilizing the general framework in [33], we propose a new algorithm that is proven to converge to at least the neighborhood of the stationary points<sup>2</sup> of the formulated problem. Here, the coupling among the variables makes it challenging to develop a specific algorithm that satisfies all the strict conditions stated in the general framework of [33]. It is also noted that our algorithm only requires channel stability in each but not all iterations. This important feature ensures the problem and its solution remain up-to-date and valid during the running time of the algorithm, despite the channel variations.
- Simulation results verify the convergence of the proposed algorithm, and show that our solution reduces the training time by up to 55% compared with the baseline schemes. They further confirm that cell-free massive MIMO offers the lowest training time compared to cell-free TDMA massive MIMO and collocated massive MIMO.

*Paper Organization and Notation:* The rest of this paper is organized as follows. Section II introduces a specific FL framework used in this paper. Section III proposes a novel scheme for cell-free massive MIMO networks to support this FL framework. Section IV presents the system model and assumptions. Section V formulates the FL training time minimization problem, whereas Section VI proposes a new algorithm to solve the formulated problem. For comparison, Section VII introduces cell-free TDMA and collocated massive MIMO systems to also support the considered FL framework. Section VIII verifies the performance of the developed algorithm through comprehensive numerical examples. Finally, Section IX concludes the paper.

In this paper, boldfaced symbols are used for vectors and capitalized boldfaced symbols for matrices.  $\mathbf{X}^*$  and  $\mathbf{X}^H$  are the conjugate and conjugate transposition of a matrix  $\mathbf{X}$ , respectively.  $\mathbb{R}^d$  is a space where its elements are real vectors with length  $d$ .  $\langle \mathbf{x}, \mathbf{y} \rangle$  means the inner product of vectors  $\mathbf{x}$  and  $\mathbf{y}$ .  $\|\cdot\|$  denotes the  $\ell_2$ -norm function.  $\mathcal{CN}(\boldsymbol{\mu}, \mathbf{Q})$  denotes the circularly symmetric complex Gaussian distribution with mean  $\boldsymbol{\mu}$  and covariance  $\mathbf{Q}$ .  $\nabla g$  is the gradient of a function  $g$ .  $\mathbb{E}\{\cdot\}$  denotes the expected value of a random variable  $x$ .

<sup>2</sup>The definition of stationary points is given in [33, Definition 1].

## II. A FEDERATED LEARNING FRAMEWORK [34]

Because of all the potential advantages offered by FL, many types of FL frameworks have so far been studied despite research on FL is still in its infancy [34]–[39]. Different network model designs may be required to support these different FL frameworks. In this section, we focus on the FL framework of [34] which can be supported by the network model proposed in the next section.

Specifically here, a global ML problem is solved at a central server with a global training data set partitioned over a large number of participating clients. Each client trains their local model by an arbitrary learning algorithm. Let  $\mathcal{K}$  be the set of clients and  $D_k$  the size of the local data stored at client  $k$ . Then  $\tilde{D} = \sum_{k \in \mathcal{K}} D_k$  is the size of the global training data. Denote by  $\mathcal{D} = \{1, \dots, \tilde{D}\}$  and  $\mathcal{D}_k = \{1, \dots, D_k\}$  the index sets of the global data samples and the local data samples at a client  $k$ , respectively. In a typical supervised learning, a data sample  $i \in \mathcal{D}$  is defined as an input-output pair  $\{\mathbf{x}_i \in \mathbb{R}^d, y_i\}$ .

For  $\lambda > 0$ , the general global ML problem can be posed as the following minimization

$$\min_{\mathbf{w} \in \mathbb{R}^d} J(\mathbf{w}) \triangleq \frac{1}{\tilde{D}} \sum_{i \in \mathcal{D}} f_i(\mathbf{w}) + \lambda g(\mathbf{w}), \quad (1)$$

where  $f_i(\mathbf{w})$  is the loss function at data sample  $i$  and  $g(\mathbf{w})$  is a regularization term with a model parameter  $\mathbf{w}$ . Some popular examples are  $f_i(\mathbf{w}) = \frac{1}{2}(\mathbf{x}_i^T \mathbf{w} - y_i)^2$  for a linear regression problem and  $f_i(\mathbf{w}) = \{0, 1 - y_i \mathbf{x}_i^T \mathbf{w}\}$ ,  $y_i \in \{-1, 1\}$  for a support vector machine. Here, the learning problem is to find  $\mathbf{w}$  that characterizes the output  $y_i$  with the loss function  $f_i(\mathbf{w})$  for a given input  $\mathbf{x}_i$ .

The dual problem of (1) is written as

$$\max_{\boldsymbol{\alpha} \in \mathbb{R}^{\tilde{D}}} J_{\tilde{D}}(\boldsymbol{\alpha}) \triangleq \frac{1}{\tilde{D}} \sum_{i \in \mathcal{D}} -f_i^*(-\boldsymbol{\alpha}) - \lambda g^*(\boldsymbol{\chi}(\boldsymbol{\alpha})), \quad (2)$$

which is a special case of the Fenchel duality [34], where  $f_i^*$  and  $g^*$  are the convex conjugate functions of  $f_i$  and  $g$ , respectively;  $\boldsymbol{\alpha}$  is a dual variable;  $\boldsymbol{\chi}(\boldsymbol{\alpha}) = \frac{1}{\lambda \tilde{D}} \mathbf{X} \boldsymbol{\alpha}$ ;  $\mathbf{X} = [\mathbf{x}_1, \dots, \mathbf{x}_{\tilde{D}}] \in \mathbb{R}^{d \times \tilde{D}}$ . It can be shown that if  $\boldsymbol{\alpha}^*$  is an optimal solution of (2), then  $\mathbf{w}(\boldsymbol{\alpha}^*) = \nabla g^*\left(\frac{1}{\lambda \tilde{D}} \mathbf{X} \boldsymbol{\alpha}^*\right)$  is the optimal solution of (1). This property allows handling the dual variable  $\boldsymbol{\alpha} \in \mathbb{R}^{\tilde{D}}$  instead of  $\mathbf{w} \in \mathbb{R}^d$ . Since each  $\alpha_i$  corresponds to each data sample  $i$ ,  $\boldsymbol{\alpha}$  can be distributed in the same way that data are partitioned for the  $K$  clients.

For any  $\boldsymbol{\phi} \in \mathbb{R}^{\tilde{D}}$ , denote by  $\boldsymbol{\phi}_{[k]} \in \mathbb{R}^{\tilde{D}}$  the vector such that  $(\boldsymbol{\phi}_{[k]})_i = \phi_i$  if  $i \in \mathcal{D}_k$  and 0 otherwise. Similarly, denote by  $\mathbf{X}_{[k]} \in \mathbb{R}^{d \times \tilde{D}}$  the matrix that includes non-zero columns  $i \in \mathcal{D}_k$  and 0 in all other columns. The local problem at each client  $k$  is then assigned to find the optimal change  $\boldsymbol{\phi}_{[k]}$  in the local dual variable  $\boldsymbol{\alpha}_{[k]}$ , for a given previous  $\boldsymbol{\alpha}$  as

$$\max_{\boldsymbol{\phi}_{[k]} \in \mathbb{R}^{\tilde{D}}} J_k(\boldsymbol{\phi}_{[k]}, \boldsymbol{\chi}(\boldsymbol{\alpha}), \boldsymbol{\alpha}_{[k]}), \quad (3)$$

where

$$\begin{aligned} J_k(\boldsymbol{\phi}_{[k]}, \boldsymbol{\chi}(\boldsymbol{\alpha}), \boldsymbol{\alpha}_{[k]}) &= \\ &= -\frac{1}{K} g^*(\boldsymbol{\chi}(\boldsymbol{\alpha})) - \left\langle \frac{1}{D} \mathbf{X}_{[k]}^T \nabla g^*(\boldsymbol{\chi}(\boldsymbol{\alpha})), \boldsymbol{\phi}_{[k]} \right\rangle \\ &\quad - \frac{1}{2} \left\| \frac{1}{\lambda \tilde{D}} \mathbf{X}_{[k]} \boldsymbol{\phi}_{[k]} \right\|^2 - \frac{1}{D} \sum_{i \in \mathcal{D}_k} f_i^*(-(\boldsymbol{\alpha}_{[k]})_i - (\boldsymbol{\phi}_{[k]})_i) \end{aligned} \quad (4)$$

### Algorithm 1 Federated learning framework [34]

---

```

1: Input: an initial point  $\boldsymbol{\alpha}^{(0)}$  and all local training data sets
2: Set  $n = 1$ ,  $\boldsymbol{\chi}^{(0)} = \frac{1}{\lambda \tilde{D}} \mathbf{X} \boldsymbol{\alpha}^{(0)}$ 
3: repeat
4:   for  $k \in \mathcal{K}$  in parallel do
5:     Solve (3) by an iterative algorithm with a local
       accuracy  $\theta$  to obtain an optimal solution  $\boldsymbol{\phi}_{[k]}^*$ 
6:     Update the local dual variable  $\boldsymbol{\alpha}_{[k]}^{(n+1)}$  by (5)
7:     Share  $\Delta \boldsymbol{\chi}_k^{(n)}$  in (6) to the central server
8:   end for
9:   Update  $\boldsymbol{\chi}^{(n+1)}$  as (7) and send it back to the clients
10:  Update  $n = n + 1$ 
11: until convergence of the global accuracy  $\epsilon$ 

```

---

is the quadratic approximation of  $J_{\tilde{D}}$  at the dual variable  $(\boldsymbol{\alpha}_{[k]} + \boldsymbol{\phi}_{[k]})$ . Here, the only information shared between the clients and the central server is the change in  $\boldsymbol{\chi}$ .

At iteration  $n$ , each client  $k \in \mathcal{K}$  solves (3) by an arbitrary iterative algorithm with a local accuracy level of  $\theta$  in order to obtain its optimal solution  $\boldsymbol{\phi}_{[k]}^*$ . The local dual variable is updated as

$$\boldsymbol{\alpha}_{[k]}^{(n+1)} = \boldsymbol{\alpha}_{[k]}^{(n)} + \boldsymbol{\phi}_{[k]}^*. \quad (5)$$

Each client  $k \in \mathcal{K}$  then shares its local change in  $\boldsymbol{\chi}^{(n)}$ , i.e.,

$$\Delta \boldsymbol{\chi}_k^{(n)} = \frac{1}{\lambda \tilde{D}} \mathbf{X}_{[k]} \boldsymbol{\phi}_{[k]}^*, \quad (6)$$

to the central server. The central server aggregates the local information  $\Delta \boldsymbol{\chi}_k^{(n)}$  received from all the clients and updates  $\boldsymbol{\chi}$  as

$$\boldsymbol{\chi}^{(n+1)} = \boldsymbol{\chi}^{(n)} + \frac{1}{K} \Delta \boldsymbol{\chi}_k^{(n)}. \quad (7)$$

$\boldsymbol{\chi}^{(n+1)}$  is finally sent back to the clients to solve (3). This process will terminate when a global accuracy level of  $\epsilon$  is reached. The FL framework described above is summarized in Algorithm 1.

**Definition 1.** *Training updates are the information shared between the central server and clients, i.e.,  $\Delta \boldsymbol{\chi}_k$  and  $\boldsymbol{\chi}$ , as shown in (6) and (7).*

**Definition 2.** *An FL process is defined as a full execution of Algorithm 1.*

We assume that each client  $k \in \mathcal{K}$  uses optimization algorithms such as stochastic average gradient (SAG) and stochastic variance reduced gradient (SVRG) to solve (3) with a local accuracy level of  $\theta$ . The number of local iterations is then [38]

$$L(\theta) = \nu \log\left(\frac{1}{\theta}\right), \quad (8)$$

where  $\nu > 0$  depends on the data size and structure of the local problem [38]. On the other hand, for strongly convex objective functions and the global accuracy level of  $\epsilon$ , the number of global iterations are given by [17], [34]

$$G(\theta) = \frac{\vartheta \log\left(\frac{1}{\epsilon}\right)}{1 - \theta}, \quad (9)$$

where  $\vartheta > 0$  and  $\epsilon$  is assumed to be known. Note that the numbers of local and global iterations may change when each client uses other optimization algorithms for local updates, and other FL frameworks are used. Assuming (8) and (9),

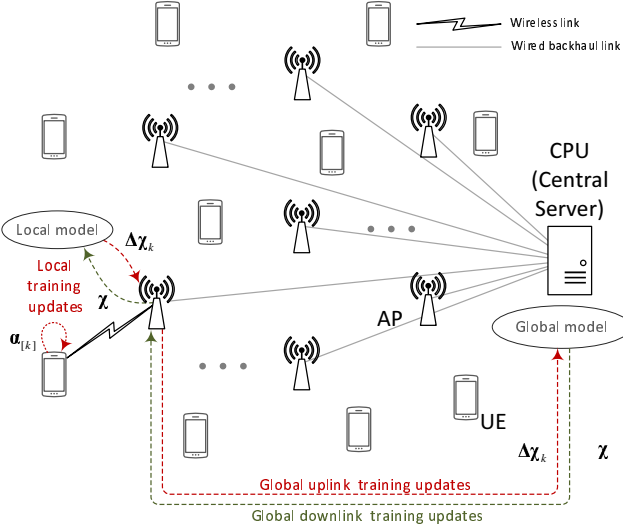


Fig. 1. A cell-free massive MIMO network model used to support FL

the system model and the optimization problem presented in the sequel are therefore only valid for the FL framework considered in this section.

### III. PROPOSED SCHEME FOR CELL-FREE MASSIVE MIMO NETWORKS TO SUPPORT FEDERATED LEARNING

#### A. The Network Model

This section proposes using the cell-free massive MIMO network structure [31] illustrated in Fig. 1 to implement the FL framework in Algorithm 1. In this structure, a central processing unit (CPU) is connected to a set of access points (APs)  $\mathcal{M} = \{1, \dots, M\}$  via backhaul links with sufficient capacities. These APs serve a set of participating UEs  $\mathcal{K} = \{1, 2, \dots, K\}$  via wireless access links at the same time and in the same frequency bands. The APs and UEs are each equipped with a single antenna. The CPU and UEs act as the central server and the clients in Algorithm 1, respectively. The APs are used to relay the training updates between the CPU and the UEs. Furthermore, we insist a functional platform is installed at the CPU to interact with the UEs via an application interface, in order to leverage FL and build a global model of ML.

An FL process described by Algorithm 1 consists of several iterations of the “REPEAT-UNTIL” loop. To implement each of these iterations by the above cell-free massive MIMO model, we propose the following four key steps.

- S1) The CPU sends a global downlink (DL) training update  $\chi$  to the UEs in order for them to update their local models.
- S2) At each UE  $k$ ,  $\alpha_k$  and  $\Delta\chi_k$  are updated by minimizing the local loss functions on their local training data sets.
- S3) The UEs send global uplink (UL) training updates  $\Delta\chi_k, \forall k$  back to the CPU.
- S4) These training updates are aggregated by the CPU to update the global training update  $\chi$ .

#### B. The Proposed Scheme

To realize the FL process in the considered cell-free massive MIMO network structure, we propose a general scheme shown in Fig. 2. As seen from the figure, we divide the time period during which the statistics of large-scale fading is stable into

multiple time intervals. The first interval of “FL performance optimization” is used for optimizing the performance of FL. The remaining intervals are reserved for the FL process; hence, termed as “FL process” intervals.

1) *Optimizing the performance of FL*: In the “FL performance optimization” interval, any algorithms can be developed to optimize the performance of FL before the FL processes are executed. Here, we denote by “system parameters” the parameters that are designed by the FL optimization algorithm. These parameters are grouped into short-term and long-term parameters. The short-term parameters change in the timescale of large-scale coherence times, whereas the long-term parameters the statistics of large-scale fading. In each iteration of the optimization algorithm, the short-term parameters are designed in the short-term optimization (STO) time blocks, whereas the long-term parameters in the long-term optimization (LTO) time blocks. As a result of the channel hardening effect in massive MIMO, the wireless channel remains unchanged during one large-scale coherence time  $\tilde{T}_c$ . In practice, the completion time of the optimization algorithm can be larger than  $\tilde{T}_c$ . Therefore, we insist that only one iteration of the algorithm is to happen within  $\tilde{T}_c$ .

2) *Implementing the FL process*: In the “FL process” intervals, the FL process is executed with the long-term parameters obtained from the “FL performance optimization” interval. The short-term parameters are optimized in the STO time block to enhance the performance of training update transmission before each iteration of the FL process. Since the completion time of the FL process can be larger than  $\tilde{T}_c$ , we insist that both STO and “one iteration of the FL process” time blocks are to happen in one  $\tilde{T}_c$ .

3) *Implementing each iteration of the FL process*: Fig. 3 shows the time block of “one iteration of the FL process”, in which the intervals of the four key steps to implement each iteration of the FL process by the cell-free massive MIMO model are illustrated. Here, the interval of Step S1) in Section III-A consists one interval of “DL training update transmission (DLTUT) via backhaul links” from the CPU to the APs, and one interval of “DLTUT via wireless links” from the APs to the UEs. The interval of Step S3) includes one interval of “UL training update transmission (ULTUT) via wireless links” from the UEs to the APs, and one interval of “ULTUT via backhaul links” from the APs to the CPU.

As also seen from Fig. 3, we split each time block of “DLTUT via wireless links” or “ULTUT via wireless links” into multiple intervals. The intervals of “UL training” is used for channel estimation. The remaining intervals are used for DL/UL training update transmission. In these “DLTUT” or “ULTUT” intervals, any beamforming/filtering design can be applied to optimize the performance of training update transmission. Here, we insist that the pair of “UL training” and “DLTUT”/“ULTUT” intervals happen in one coherence time  $T_c$  in order to adapt to the variation of small-scale fading. In addition, the data size of training updates may be larger than the amount of data that can be transmitted in  $T_c$ . As such, there may be one or several “DLTUT” or “ULTUT” intervals in each “DLTUT via wireless links” or “ULTUT via wireless links” time block in order to complete the transmission of one

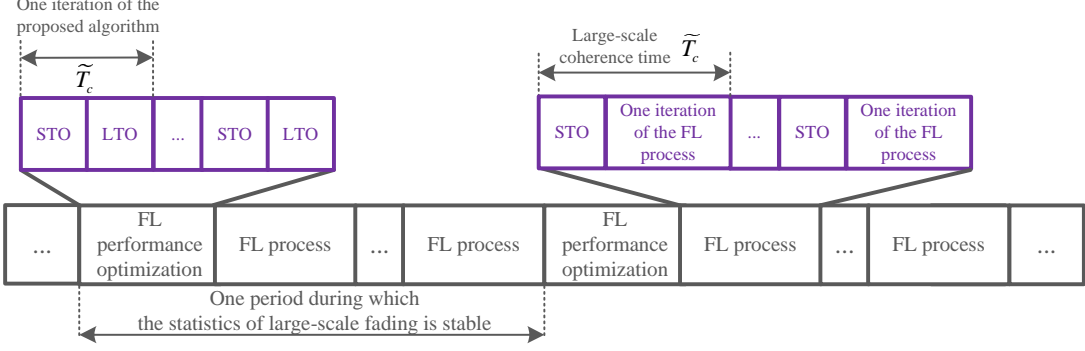


Fig. 2. Designed scheme of a cell-free massive MIMO system to support FL

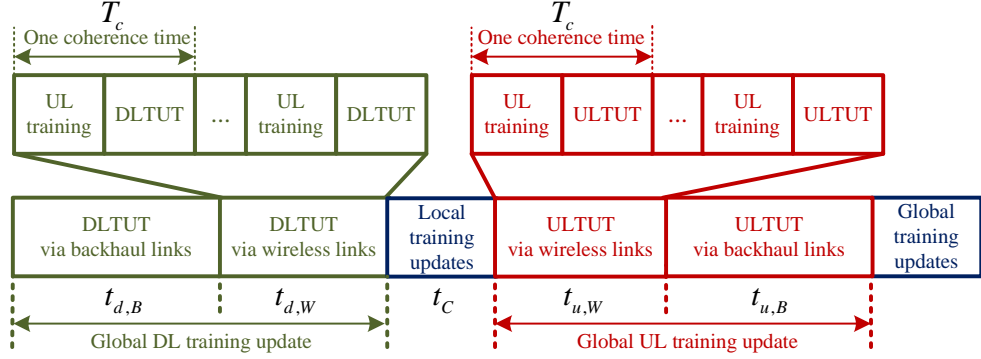


Fig. 3. One iteration of the FL process

global DL/UL training update.

#### IV. OPTIMIZATION OF FL PERFORMANCE: DETAILED SYSTEM MODEL

This section details the cell-free massive MIMO system model used to support the transmission and computation of the training updates in one iteration of the FL process (see Fig. 3).

##### A. The Model of Training Update Transmission

1) *UL Training for Channel Estimation*: Denote by  $\tau_c = T_c B_c$  the number of samples of each coherence block, where  $T_c$  is the coherence time and  $B_c$  the coherence bandwidth. The training pilot sequences are sent by all the UEs to all the APs simultaneously. Denote by  $\tau_t$  (samples) the length of one pilot sequence. Let  $\sqrt{\tau_t} \varphi_k \in \mathbb{C}^{\tau_t \times 1}$  be the pilot sequence transmitted from UE  $k \in \mathcal{K}$ , where  $\|\varphi_k\|^2 = 1, \forall k \in \mathcal{K}$ . The channel from a UE  $k$  to an AP  $m$  is modeled as

$$g_{mk} = (\beta_{mk})^{1/2} \tilde{g}_{mk}, \quad (10)$$

where  $\beta_{mk}$  and  $\tilde{g}_{mk} \in \mathbb{C}$  represent the large-scale fading and small-scale fading channel coefficients, respectively. Assume that  $\tilde{g}_{mk}$  is an independent and identically distributed (i.i.d.)  $\mathcal{CN}(0, 1)$  random variable.

The AP  $m$  receives the following pilot vector

$$\mathbf{y}_m = \sqrt{\tau_t \rho_t} \sum_{k \in \mathcal{K}} g_{mk} \varphi_k + \mathbf{w}_m, \quad (11)$$

where  $\rho_t$  is the normalized signal-to-noise ratio (SNR) of each pilot symbol, and  $\mathbf{w}_m \in \mathcal{CN}(\mathbf{0}, \mathbf{I})$  is the additive noise at the AP  $m$ . The projection of  $\mathbf{y}_m$  onto  $\varphi_k$  is given as

$$\hat{y}_m = \varphi_k^H \mathbf{y}_m = \sqrt{\tau_t \rho_t} \sum_{\ell \in \mathcal{K}} g_{m\ell} \varphi_k^H \varphi_\ell + \varphi_k^H \mathbf{w}_m. \quad (12)$$

After receiving  $\hat{y}_m$ , the AP  $m$  estimates  $g_{mk}$  by using the minimum mean-square error (MMSE) estimation. Given  $\hat{y}_m$ , the MMSE estimate  $\hat{g}_{mk}$  of  $g_{mk}$  is obtained as [40]

$$\hat{g}_{mk} = \mathbb{E}\{\hat{y}_m^* g_{mk}\} (\mathbb{E}\{|\hat{y}_m|^2\})^{-1} \hat{y}_m = c_{mk} \hat{y}_m, \quad (13)$$

where  $c_{mk} \triangleq \frac{\sqrt{\tau_t \rho_t} \beta_{mk}}{\sum_{\ell \in \mathcal{K}} \tau_t \rho_t \beta_{m\ell} |\varphi_k^H \varphi_\ell|^2 + 1}$ . From the property of MMSE channel estimation,  $\hat{g}_{mk}$  is distributed according to  $\mathcal{CN}(0, \sigma_{mk}^2)$ , where  $\sigma_{mk}^2 = \frac{\tau_t \rho_t (\beta_{mk})^2}{\sum_{\ell \in \mathcal{K}} \tau_t \rho_t \beta_{m\ell} |\varphi_k^H \varphi_\ell|^2 + 1}$  [40].

*Remark 1.* In indoor communications, the time for UL training can be much smaller than the coherence time  $T_c$ . For example, a system supporting users' mobility of  $v = 0.75$  m/s = 2.7 km/h, delay spread of  $T_d = 0.5$   $\mu$ s and carrier frequency  $f_c = 2$  GHz has a coherence time of  $T_c = \frac{c}{4f_c v} = 50$  ms, and coherence bandwidth  $B_c = \frac{1}{2T_d} = 1$  MHz [41]. Suppose  $\tau_t = 20$ , the UL training time is  $t_t = \frac{\tau_t}{B_c} = 0.02$  ms  $\ll T_c$ . Therefore, the UL training time can be ignored in one coherence time and one FL process interval.

2) *Global DL Training Update*: At the CPU, the global training update  $\chi$  intended for a UE  $k$  is encoded into a symbol  $s_{d,k} \sim \mathcal{CN}(0, 1)$ . Then the CPU sends  $s_{d,k}, \forall k \in \mathcal{K}$ , to all the APs over backhaul links. Let  $S_d$  (bits) and  $R_{d,k}$  (bps) be the data size and the data rate of the global DL training update for the UE  $k$ , respectively. The download latency from the CPU to all the APs is given by

$$t_{d,B}(\mathbf{R}_d) = \frac{KS_d}{\sum_{k \in \mathcal{K}} R_{d,k}}, \quad (14)$$

where  $\mathbf{R}_d \triangleq \{R_{d,k}\}_{k \in \mathcal{K}}$ .

For ease of implementation, we apply a conjugate beamforming scheme to the APs to precode the message signals

before wirelessly transmitting them to the UEs (using the channel estimates from the UL training). The transmitted signal at an AP  $m$  is expressed as

$$x_{d,m} = \sqrt{\rho_d} \sum_{k \in \mathcal{K}} \sqrt{\eta_{mk}} (\hat{g}_{mk})^* s_{d,k}, \quad (15)$$

where  $\rho_d$  is the maximum normalized transmit power at each AP and  $\eta_{mk}, \forall m \in \mathcal{M}, k \in \mathcal{K}$ , is a power control coefficient. The AP  $m$  is required to meet the average normalized power constraint, i.e.,  $\mathbb{E}\{|x_{d,m}|^2\} \leq \rho_d$ , which can also be expressed as the following per-AP power constraint:

$$\sum_{k \in \mathcal{K}} \sigma_{mk}^2 \eta_{mk} \leq 1, \forall m. \quad (16)$$

The received signal at the UE  $k$  is given by

$$\begin{aligned} r_{d,k} &= \sum_{m \in \mathcal{M}} g_{mk} x_{d,m} + w_k \\ &= \sqrt{\rho_d} \sum_{m \in \mathcal{M}} \sqrt{\eta_{mk}} g_{mk} (\hat{g}_{mk})^* s_{d,k} \\ &\quad + \sqrt{\rho_d} \sum_{m \in \mathcal{M}} \sum_{\ell \in \mathcal{K} \setminus \{k\}} \sqrt{\eta_{m\ell}} g_{mk} (\hat{g}_{m\ell})^* s_{d,\ell} + w_k, \end{aligned} \quad (17)$$

where  $w_k$  is the additive noise  $\mathcal{CN}(0, 1)$  at the UE  $k$ . The achievable DL rate at the UE  $k$  is

$$R_{d,k} \leq h_{d,k}(\boldsymbol{\eta}), \quad (18)$$

where  $\boldsymbol{\eta} \triangleq \{\eta_{mk}\}_{m \in \mathcal{M}, k \in \mathcal{K}}$  and  $h_{d,k}(\boldsymbol{\eta})$  is given in (19) shown at the top of the next page [31]. Note that in (19),  $B$  is the bandwidth. The download latency from the APs to the UE  $k$  is given by

$$t_{d,k}(R_{d,k}) = \frac{S_d}{R_{d,k}}. \quad (20)$$

3) *Global UL Training Update:* After updating the local model, the UE  $k$  encodes the global UL training update  $\Delta \chi_k$  into a symbol  $s_{u,k} \sim \mathcal{CN}(0, 1)$ . The symbol  $s_{u,k}$  is then allocated a transmit amplitude value  $\sqrt{\rho_u \zeta_k}$  to generate a baseband signal  $x_{u,k}$  for wireless transmissions, i.e.,  $x_{u,k} = \sqrt{\rho_u \zeta_k} s_{u,k}$ . The UE  $k$  is adhered to the average transmit power constraint, i.e.,  $\mathbb{E}\{|x_{u,k}|^2\} \leq \rho_u$ , which can also be expressed in a per-UE constraint as

$$0 \leq \zeta_k \leq 1, \forall k \in \mathcal{K}. \quad (21)$$

The upload latency from the UE  $k$  to the AP  $m$  is given by

$$t_{u,k}(R_{u,k}) = \frac{S_u}{R_{u,k}}, \quad (22)$$

where  $S_u$  (bits) and  $R_{u,k}$  (bps) are the data size and the data rate of the global UL training update, respectively.

The received signal at the AP  $m$  is expressed as

$$\begin{aligned} y_{u,m} &= \sum_{k \in \mathcal{K}} g_{mk} x_{u,k} + w_{u,m} \\ &= \sqrt{\rho_u} \sum_{k \in \mathcal{K}} g_{mk} \sqrt{\zeta_k} s_{u,k} + w_{u,m}, \end{aligned} \quad (23)$$

where  $w_{u,m} \sim \mathcal{CN}(0, 1)$  is the additive noise. To detect the message symbol transmitted from the UE  $k$ , the AP  $m$  computes and sends  $(\hat{g}_{mk})^* y_{u,m}$  to the CPU. The upload latency from the APs to the CPU is expressed as

$$t_{u,B}(\mathbf{R}_u) = \frac{KS_u}{\sum_{k \in \mathcal{K}} R_{u,k}} \quad (24)$$

where  $\mathbf{R}_u \triangleq \{R_{u,k}\}_{k \in \mathcal{K}}$ .

At the CPU, the symbol  $s_{u,\ell}$  is detected from the received signal  $r_{u,k}$ :

$$\begin{aligned} r_{u,k} &= \sqrt{\rho_u} \sum_{m \in \mathcal{M}} \sqrt{\zeta_k} (\hat{g}_{mk})^* g_{mk} s_{u,k} \\ &\quad + \sqrt{\rho_u} \sum_{m \in \mathcal{M}} \sum_{\ell \in \mathcal{K} \setminus \{k\}} \sqrt{\zeta_\ell} (\hat{g}_{mk})^* g_{m\ell} s_{u,\ell} \\ &\quad + \sum_{m \in \mathcal{M}} (\hat{g}_{mk})^* w_{u,m}. \end{aligned} \quad (25)$$

The achievable UL rate for the UE  $k$  is given by

$$R_{u,k} \leq h_{u,k}(\boldsymbol{\zeta}), \quad (26)$$

where  $\boldsymbol{\zeta} \triangleq \{\zeta_k\}_{k \in \mathcal{K}}$  and  $h_{u,k}(\boldsymbol{\zeta})$  is defined in (27) shown at the top of the next page [31].

### B. The Model of Local Training Update Computation at UEs

Denote by  $c_k$  (cycles/sample) the number of processing cycles for a UE  $k$  to process one data sample.  $c_k$  is known *a priori* by an offline measurement [42]. Let  $D_k$  (samples) and  $f_k$  (cycles/s) be the size of the local data set and the processing frequency of the UE  $k$ , respectively. The latency of computing the local training update at the UE  $k$  is by

$$t_{C,k}(\theta, f_k) = \frac{D_k c_k}{f_k}, \quad (28)$$

where  $L(\theta)$  is the number of local training iterations (see (8)) and  $\frac{D_k c_k}{f_k}$  is the time taken to compute the local update over its local training data set in each iteration. Given the limited computational resource at the UEs, we only focus on the delay of computing the local updates at the UEs. Since the computational resource of the CPU is much more abundant than that of the UEs, the latency of aggregating the global UL training updates at the CPU is negligible, and hence ignored.

### C. The Model of UE's Energy Consumption

Because the time of UL training for channel estimation is negligible compared with one FL training interval, the energy consumed in the time block of UL training is ignored. The energy consumption in the time block of UL training at a UE  $k$  is given by

$$E_{T,k}(\zeta_k, R_{u,k}) = \zeta_k \frac{S_u}{R_{u,k}}, \quad (29)$$

where  $\zeta_k$  is the transmitted UL power and  $\frac{S_u}{R_{u,k}}$  is the delay incurred by transmitting the global UL training update  $\Delta \chi_k$ . The energy required for computing local training updates at the UE  $k$  is expressed as [18]

$$E_{C,k}(\theta, f_k) = L(\theta) \frac{\alpha}{2} c_k D_k f_k^2, \quad (30)$$

where  $\frac{\alpha}{2}$  is the effective capacitance coefficient of the UEs' computing chipset.

## V. FL TRAINING TIME MINIMIZATION: PROBLEM FORMULATION

To optimize the performance of the FL process in the cell-free massive MIMO network model discussed in Sections III and IV, this paper targets the key performance metric of *training time minimization*.

The time of one global DL training update for a UE  $k$  involves the transmission delay of sending the global DL training update from the CPU to the APs via backhaul links and that from the APs to UE  $k$  via wireless links, i.e.,

$$h_{d,k}(\boldsymbol{\eta}) = \frac{\tau_c - \tau_t}{\tau_c} B \log_2 \left( 1 + \frac{\rho_d \left( \sum_{m \in \mathcal{M}} \eta_{mk}^{1/2} \sigma_{mk}^2 \right)^2}{\rho_d \sum_{\ell \in \mathcal{K} \setminus k} \left( \sum_{m \in \mathcal{M}} \eta_{m\ell}^{1/2} \sigma_{m\ell}^2 \frac{\beta_{mk}}{\beta_{m\ell}} \right)^2 |\boldsymbol{\varphi}_\ell^H \boldsymbol{\varphi}_k|^2 + \rho_d \sum_{\ell \in \mathcal{K}} \sum_{m \in \mathcal{M}} \eta_{m\ell} \sigma_{m\ell}^2 \beta_{mk} + 1} \right) \quad (19)$$

$$h_{u,k}(\boldsymbol{\zeta}) = \frac{\tau_c - \tau_t}{\tau_c} B \log_2 \left( 1 + \frac{\rho_u \zeta_k \left( \sum_{m \in \mathcal{M}} \sigma_{mk}^2 \right)^2}{\rho_u \sum_{\ell \in \mathcal{K} \setminus k} \zeta_\ell \left( \sum_{m \in \mathcal{M}} \sigma_{mk}^2 \frac{\beta_{m\ell}}{\beta_{mk}} \right)^2 |\boldsymbol{\varphi}_k^H \boldsymbol{\varphi}_\ell|^2 + \rho_u \sum_{\ell \in \mathcal{K}} \zeta_\ell \sum_{m \in \mathcal{M}} \sigma_{mk}^2 \beta_{m\ell} + \sum_{m \in \mathcal{M}} \sigma_{mk}^2} \right) \quad (27)$$

$$t_{T,k}^d(\mathbf{R}_d) = t_{d,B}(\mathbf{R}_d) + t_{d,k}(R_{d,k}) = \frac{KS_d}{\sum_{k \in \mathcal{K}} R_{d,k}} + \frac{S_d}{R_{d,k}}. \quad (31)$$

Similarly, the time of one global UL training update from UE  $k$  consists of the delay of transmitting the global UL training update from UE  $k$  to the APs and from the APs to the CPU, i.e.,

$$t_{T,k}^u(\mathbf{R}_u) = t_{u,k}(R_{u,k}) + t_{u,B}(\mathbf{R}_u) = \frac{S_u}{R_{u,k}} + \frac{KS_u}{\sum_{k \in \mathcal{K}} R_{u,k}}. \quad (32)$$

As shown in Fig. 3, one iteration of the FL process involves the four steps of global DL training update, local training updates computed at the UEs, global UL training update and one global training update at the CPU. In the scheme developed in Section III, each of these steps must be completed for all UEs before the latter step is executed. Therefore, the time of one iteration of the FL process is

$$\begin{aligned} T_G(\theta, \mathbf{f}, \mathbf{R}_d, \mathbf{R}_u) &= \max_{k \in \mathcal{K}} t_{T,k}^d(\mathbf{R}_d) + \max_{k \in \mathcal{K}} t_{C,k}(\theta, f_k) + \max_{k \in \mathcal{K}} t_{T,k}^u(\theta, \mathbf{f}, \mathbf{R}_u) \\ &= t_{d,B}(\mathbf{R}_d) + \max_{k \in \mathcal{K}} t_{d,k}(R_{d,k}) + \max_{k \in \mathcal{K}} t_{C,k}(\theta, f_k) \\ &\quad + \max_{k \in \mathcal{K}} t_{u,k}(R_{u,k}) + t_{u,B}(\mathbf{R}_u) \\ &\triangleq t_{d,B} + t_{d,W} + t_C + t_{u,W} + t_{u,B}, \end{aligned} \quad (33)$$

where  $\mathbf{f} \triangleq \{f_k\}_{k \in \mathcal{K}}$ ;  $t_{d,W}$  or  $t_{u,W}$  is the maximum delay for a complete DLTUT or ULTUT via wireless links;  $t_C$  is the maximum delay for all the UEs to complete their local training update computation. Note again that the time of the global training update at the CPU is ignored as discussed in Section IV-B.

As can be seen from (33),  $T_G(\theta, \mathbf{f}, \mathbf{R}_d, \mathbf{R}_u)$  relies on both  $(\mathbf{f}, \mathbf{R}_d, \mathbf{R}_u)$  and  $\theta$ . However, only  $(\mathbf{f}, \mathbf{R}_d, \mathbf{R}_u)$  is optimized to reduce the time  $T_G(\theta, \mathbf{f}, \mathbf{R}_d, \mathbf{R}_u)$  of one iteration of the FL process in each large-scale coherence time. This is because any change of  $\theta$  leads to the change in the number of iterations  $G(\theta)$  of the FL process as shown in (9). Therefore,  $(\mathbf{f}, \mathbf{R}_d, \mathbf{R}_u)$  and  $\theta$  must be optimized independently in different timescales.

To measure how efficient the time of each iteration of the FL process is optimized over different large-scale coherence times, we introduce a new metric termed ‘‘ergodic time of one iteration of the FL process’’, i.e.,  $\mathbb{E}\{T_G(\theta, \mathbf{f}, \mathbf{R}_d, \mathbf{R}_u)\}$ . Here,  $\mathbb{E}\{T_G(\theta, \mathbf{f}, \mathbf{R}_d, \mathbf{R}_u)\}$  is the average of  $T_G(\theta, \mathbf{f}, \mathbf{R}_d, \mathbf{R}_u)$  over the large-scale fading realizations. The effective time of one FL process is then defined as

$$\begin{aligned} T_e(\theta, \mathbf{f}, \mathbf{R}_d, \mathbf{R}_u) &\triangleq G(\theta) \mathbb{E}\{T_G(\theta, \mathbf{f}, \mathbf{R}_d, \mathbf{R}_u)\} \\ &= \vartheta \log\left(\frac{1}{\epsilon}\right) \mathbb{E}\left\{\frac{T_G(\theta, \mathbf{f}, \mathbf{R}_d, \mathbf{R}_u)}{1 - \theta}\right\} \\ &\triangleq \vartheta \log\left(\frac{1}{\epsilon}\right) \mathbb{E}\{T(\theta, \mathbf{f}, \mathbf{R}_d, \mathbf{R}_u)\}. \end{aligned} \quad (34)$$

For ease of presentation, we make the following definition.

**Definition 3.** *An effective training time of FL is the effective time of one FL process and is computed as (34).*

The problem of FL training time minimization for the considered cell-free massive MIMO system model is thus formulated as:

$$\min_{\boldsymbol{\eta}, \boldsymbol{\zeta}, \theta, \mathbf{f}, \mathbf{R}_d, \mathbf{R}_u} g(\theta, \mathbf{f}, \mathbf{R}_d, \mathbf{R}_u) \triangleq \mathbb{E}\{T(\theta, \mathbf{f}, \mathbf{R}_d, \mathbf{R}_u)\} \quad (35a)$$

$$\text{s.t. (16), (18), (21), (26)}$$

$$E_{T,k}(\zeta_k, R_{u,k}) + E_{C,k}(\theta, f_k) \leq E_{k,\max}, \forall k \quad (35b)$$

$$f_{k,\min} \leq f_k \leq f_{k,\max}, \forall k \quad (35c)$$

$$0 \leq \eta_{mk}, \forall m, k \quad (35d)$$

$$0 \leq \zeta_k, \forall k \quad (35e)$$

$$0 \leq R_{d,k}, \forall k \quad (35f)$$

$$0 \leq R_{u,k}, \forall k \quad (35g)$$

$$\theta_{\min} \leq \theta \leq \theta_{\max}. \quad (35h)$$

Problem (35) has a nonconvex stochastic, mixed-timescale structure, along with the tight coupling among the variables. Finding its globally optimal solution is challenging. This paper instead aims to propose a solution approach that is suitable for practical implementation.

## VI. FL TRAINING TIME MINIMIZATION: PROPOSED ALGORITHM

To resolve problem (35), we utilize the online successive convex approximation approach for solving two-stage stochastic nonconvex optimization problems in [33]. Note that while [33] only provides a general description of the solution method, we specifically tailor it to devise a new algorithm for (35).

According to [43], problem (35) can be decomposed into a family of short-term subproblems and a long-term master problem as follows. For a given  $\theta$  and large-scale fading coefficients  $\boldsymbol{\beta} \triangleq \{\beta_{mk}\}_{m \in \mathcal{M}, k \in \mathcal{K}}$  in each large-scale coherence time, the short-term subproblem is expressed as:

$$\min_{\boldsymbol{\eta}, \boldsymbol{\zeta}, \mathbf{f}, \mathbf{R}_d, \mathbf{R}_u} T(\mathbf{f}, \mathbf{R}_d, \mathbf{R}_u) \quad (36)$$

$$\text{s.t. (16), (18), (21), (26), (35b) – (35g).}$$

For given optimal solutions  $\{(\boldsymbol{\eta}^*, \boldsymbol{\zeta}^*, \mathbf{f}^*, \mathbf{R}_d^*, \mathbf{R}_u^*)\}$  to problems (36) at all large-scale coherence times, the long-term master problem is expressed as:

$$\begin{aligned} \min_{\theta} g(\theta) &\triangleq \mathbb{E}\{T(\theta)\} \\ \text{s.t. } (35h). \end{aligned} \quad (37)$$

### A. Solving the Short-term Subproblem (36)

It can be shown that (36) is equivalent to

$$\min_{\mathbf{x}} \frac{\omega}{1-\theta} \quad (38a)$$

$$\begin{aligned} \text{s.t. } \omega &\geq t_{d,B}(\mathbf{R}_d) + \max_{k \in \mathcal{K}} t_{d,k}(R_{d,k}) + \max_{k \in \mathcal{K}} t_{C,k}(\theta, f_k) \\ &\quad + \max_{k \in \mathcal{K}} t_{u,k}(R_{u,k}) + t_{u,B}(\mathbf{R}_u) \end{aligned} \quad (38b)$$

(16), (18), (21), (26), (35b) – (35g),

where  $\mathbf{x} \triangleq (\boldsymbol{\eta}, \boldsymbol{\zeta}, \mathbf{f}, \mathbf{R}_d, \mathbf{R}_u, \omega)$ . If we let  $\mathbf{v} \triangleq \{v_{mk}\}_{m \in \mathcal{M}, k \in \mathcal{K}}$  and  $\mathbf{u} \triangleq \{u_k\}_{k \in \mathcal{K}}$  with

$$v_{mk} \triangleq \eta_{mk}^{1/2}, \forall m, k \quad (39)$$

$$u_k \triangleq \zeta_k^{1/2}, \forall k, \quad (40)$$

then (38) can be rewritten as:

$$\min_{\tilde{\mathbf{x}}} \frac{\omega}{1-\theta} \quad (41a)$$

$$\text{s.t. } \omega \geq \frac{KS_d}{\sum_{k \in \mathcal{K}} R_{d,k}} + t_d + t_C + t_u + \frac{KS_u}{\sum_{k \in \mathcal{K}} R_{u,k}} \quad (41b)$$

$$t_d \geq \frac{S_d}{R_{d,k}}, \forall k \quad (41c)$$

$$t_C \geq \frac{\nu \log\left(\frac{1}{\theta}\right) D_k c_k}{f_k}, \forall k \quad (41d)$$

$$t_u \geq \frac{S_u}{R_{u,k}}, \forall k \quad (41e)$$

$$\varrho_k S_u + \nu \log\left(\frac{1}{\theta}\right) \frac{\alpha}{2} c_k D_k f_k^2 \leq E_{k,\max}, \forall k \quad (41f)$$

$$u_k^2 \leq \varrho_k R_{u,k}, \forall k \quad (41g)$$

$$R_{d,k} \leq h_{d,k}(\mathbf{v}) \quad (41h)$$

$$R_{u,k} \leq h_{u,k}(\mathbf{u}) \quad (41i)$$

$$\sum_{k \in \mathcal{K}} \sigma_{mk}^2 v_{mk}^2 \leq 1, \forall m \quad (41j)$$

$$0 < v_{mk}, \forall m \in \mathcal{M}, k \in \mathcal{K} \quad (41k)$$

$$0 < u_k \leq 1, \forall k \in \mathcal{K} \quad (41l)$$

(35c) – (35g),

where  $\tilde{\mathbf{x}} = \{\mathbf{x}, \mathbf{v}, \mathbf{u}, \boldsymbol{\varrho}, t_d, t_C, t_u\} \setminus \{\boldsymbol{\eta}, \boldsymbol{\zeta}\}$ ,  $\boldsymbol{\varrho} \triangleq \{\varrho_k\}_{k \in \mathcal{K}}, t_d, t_C$  and  $t_u$  are additional variables. Note that (41) is still challenging due to the nonconvex constraints (41g), (41h), and (41i).

To solve (41), we first rewrite (41g) as

$$z_k(u_k, \varrho_k, R_{u,k}) \leq 0, \forall k. \quad (42)$$

where  $z_k(u_k, \varrho_k, R_{u,k}) \triangleq 4u_k^2 - (\varrho_k + R_{u,k})^2 + (\varrho_k - R_{u,k})^2$ .

Note that, for a given point  $(x^{(n)}, y^{(n)})$ , a function  $f(x, y) = -(x+y)^2$  has an upper bound

$$\begin{aligned} \tilde{f}(x, y) &\triangleq -2(x^{(n)} + y^{(n)})(x+y) + (x^{(n)} + y^{(n)})^2 \\ &\quad + \delta((x-x^{(n)})^2 + (y-y^{(n)})^2) \geq f(x, y), \end{aligned} \quad (43)$$

where  $\delta > 0$  can be any constant. Different from the upper bound used in [44],  $\tilde{f}(x, y)$  is introduced here with the term of  $\delta((x-x^{(n)})^2 + (y-y^{(n)})^2)$  to ensure its strong convexity. Now, (41g) can be approximated at iteration  $n+1$  by the following convex constraint

$$\tilde{z}_k(u_k, \varrho_k, R_{u,k}) \leq 0, \forall k. \quad (44)$$

where

$$\begin{aligned} \tilde{z}_k(u_k, \varrho_k, R_{u,k}) &\triangleq 4u_k^2 - 2(\varrho_k^{(n)} + R_{u,k}^{(n)})(\varrho_k + R_{u,k}) \\ &\quad + (\varrho_k^{(n)} + R_{u,k}^{(n)})^2 + (\varrho_k - R_{u,k})^2 \\ &\quad + \delta((\varrho_k - \varrho_k^{(n)})^2 + (R_{u,k} - R_{u,k}^{(n)})^2). \end{aligned} \quad (45)$$

To deal with (41h) and (41i), we note that a function  $f(x, y) = \log\left(1 + \frac{|x|^2}{y}\right)$  has the following lower bound [45], [46]:

$$\begin{aligned} f(x, y) &\geq \log\left(1 + \frac{|x^{(n)}|^2}{y^{(n)}}\right) - \frac{|x^{(n)}|^2}{y^{(n)}} + 2\frac{x^{(n)}x}{y^{(n)}} \\ &\quad - \frac{|x^{(n)}|^2(|x|^2 + y)}{y^{(n)}(|x^{(n)}|^2 + y^{(n)})}, \end{aligned} \quad (46)$$

where  $x \in \mathbb{R}, y > 0, y^{(n)} > 0$ . Therefore, the concave lower bound  $\tilde{h}_{d,k}(\mathbf{v})$  of  $h_{d,k}(\mathbf{v})$  in (41h) is given by

$$\begin{aligned} \tilde{h}_{d,k}(\mathbf{v}) &\triangleq \log_2\left(1 + \frac{(\Upsilon_k^{(n)})^2}{\Pi_k^{(n)}}\right) - \frac{(\Upsilon_k^{(n)})^2}{\Pi_k^{(n)}} \\ &\quad + 2\frac{\Upsilon_k^{(n)}\Upsilon_k}{\Pi_k^{(n)}} - \frac{(\Upsilon_k^{(n)})^2(\Upsilon_k^2 + \Pi_k)}{\Pi_k^{(n)}((\Upsilon_k^{(n)})^2 + \Pi_k^{(n)})} \leq h_{d,k}(\mathbf{v}), \end{aligned} \quad (47)$$

where

$$\Upsilon_k(\{v_{mk}\}_{m \in \mathcal{M}}) = \sqrt{\rho_d} \sum_{m \in \mathcal{M}} v_{mk} \sigma_{mk}^2, \quad (48)$$

$$\begin{aligned} \Pi_k(\mathbf{v}) &= \rho_d \sum_{\ell \in \mathcal{K} \setminus k} \left( \sum_{m \in \mathcal{M}} v_{m\ell} \sigma_{m\ell}^2 \frac{\beta_{mk}}{\beta_{m\ell}} \right)^2 |\boldsymbol{\varphi}_\ell^H \boldsymbol{\varphi}_k|^2 \\ &\quad + \rho_d \sum_{\ell \in \mathcal{K}} \sum_{m \in \mathcal{M}} v_{m\ell}^2 \sigma_{m\ell}^2 \beta_{mk} + 1. \end{aligned} \quad (49)$$

Similarly, the concave lower bound  $\tilde{h}_{u,k}(\mathbf{u})$  of  $h_{u,k}(\mathbf{u})$  in (41i) is given by

$$\begin{aligned} \tilde{h}_{u,k}(\mathbf{u}) &\triangleq \log_2\left(1 + \frac{(\Psi_k^{(n)})^2}{\Xi_k^{(n)}}\right) - \frac{(\Psi_k^{(n)})^2}{\Xi_k^{(n)}} + \\ &\quad 2\frac{\Psi_k^{(n)}\Psi_k}{\Xi_k^{(n)}} - \frac{(\Psi_k^{(n)})^2(\Psi_k^2 + \Xi_k)}{\Xi_k^{(n)}((\Psi_k^{(n)})^2 + \Xi_k^{(n)})} \leq h_{u,k}(\mathbf{u}), \end{aligned} \quad (50)$$

where

$$\Psi_k(u_k) = \rho_u^{1/2} u_k \left( \sum_{m \in \mathcal{M}} \sigma_{mk}^2 \right), \quad (51)$$

$$\begin{aligned} \Xi_k(\mathbf{u}) &= \rho_u \sum_{\ell \in \mathcal{K} \setminus k} u_\ell^2 \left( \sum_{m \in \mathcal{M}} \sigma_{mk}^2 \frac{\beta_{mk}}{\beta_{m\ell}} \right)^2 |\boldsymbol{\varphi}_k^H \boldsymbol{\varphi}_\ell|^2 \\ &\quad + \rho_u \sum_{\ell \in \mathcal{K}} u_\ell^2 \sum_{m \in \mathcal{M}} \sigma_{mk}^2 \beta_{m\ell} + \sum_{m \in \mathcal{M}} \sigma_{mk}^2. \end{aligned} \quad (52)$$

As such, (41h) and (41i) can be approximated by

$$R_{d,k} \leq \tilde{h}_{d,k}(\mathbf{v}), \forall k \in \mathcal{K}, \quad (53)$$

$$R_{u,k} \leq \tilde{h}_{u,k}(\mathbf{u}), \forall k \in \mathcal{K}. \quad (54)$$

At the iteration  $n+1$ , for a given point  $\tilde{\mathbf{x}}^{(n)}$ , problem (41) (hence (36)) can finally be approximated by the following convex problem:

$$\min_{\tilde{\mathbf{x}} \in \tilde{\mathcal{F}}} \frac{\omega}{1-\theta}, \quad (55)$$

**Algorithm 2** Solving the short-term subproblem (36)

- 1: **Initialization:** Set  $n = 1$  and choose a random point  $\tilde{\mathbf{x}}^{(0)} \in \mathcal{F}$ .
- 2: **repeat**
- 3:   Update  $n = n + 1$
- 4:   Solving (55) to get its optimal solution  $\tilde{\mathbf{x}}^*$
- 5:   Update  $\tilde{\mathbf{x}}^{(n)} = \tilde{\mathbf{x}}^*$
- 6: **until** convergence

**Output:**  $(\boldsymbol{\eta}^*, \boldsymbol{\zeta}^*, \mathbf{f}^*, \mathbf{R}_d^*, \mathbf{R}_u^*)$

where  $\tilde{\mathcal{F}} \triangleq \{(35c) - (35g), (41b) - (41f), (41j) - (41l), (44), (53), (54)\}$  is a convex feasible set.

In Algorithm 2, we outline the main steps to solve problem (36). Let  $\mathcal{F} \triangleq \{(35c) - (35g), (41b) - (41l)\}$  be the feasible set of (41). Starting from a random point  $\tilde{\mathbf{x}} \in \mathcal{F}$ , we solve (55) to obtain its optimal solution  $\tilde{\mathbf{x}}^*$ . This solution is then used as an initial point in the next iteration. The algorithm terminates when an accuracy level of  $\varepsilon$  is reached. It can be confirmed that  $\tilde{h}_{d,k}(\mathbf{v})$  and  $\tilde{h}_{u,k}(\mathbf{u})$  satisfy the key properties of general inner approximation functions [47, Properties (i), (ii), and (iii)]. Therefore, Algorithm 2 converges to a Karush-Kuhn-Tucker (KKT) solution of (41) when starting from a point  $\tilde{\mathbf{x}}^{(0)} \in \mathcal{F}$  [47, Theorem 1]. By using the variable transformations (39) and (40), it can be seen that the KKT solutions of (41) satisfy the KKT conditions of (38) as well as of (36).

**B. Solving the Long-term Master Problem (37)**

At the large-scale coherence time  $n+1$ , we replace the cost function of the stochastic nonconvex problem (37) by a sample surrogate function as [33]

$$\tilde{g}^{(n+1)}(\theta) = (1 - \phi^{(n+1)})\tilde{g}^{(n)}(\theta) + \phi^{(n+1)}\tilde{T}(\theta), \quad (56)$$

where  $\phi^{(n+1)}$  is a weighting parameter.  $\tilde{g}^{(n+1)}(\theta)$  depends on the surrogate function  $\tilde{g}^{(n)}(\theta)$  of the previous large-scale coherence time  $(n)$  and the approximate function  $\tilde{T}(\theta)$  of  $T(\theta)$ . Here,  $\tilde{g}^{(n)}(\theta)$  is approximately updated as

$$\tilde{g}^{(n)}(\theta) = g^{(n)} + (\nabla g)^{(n)}(\theta - \theta^{(n+1)}), \quad (57)$$

and  $\tilde{T}(\theta)$  is expressed as

$$\tilde{T}(\theta) = T^{(n+1)} + (\nabla T)^{(n+1)}(\theta - \theta^{(n+1)}) + \tau(\theta - \theta^{(n+1)})^2, \quad (58)$$

where  $\tau > 0$  can be any constant.

With (57) and (58), (56) can be rewritten as:

$$\begin{aligned} \tilde{g}^{(n+1)}(\theta) &= g^{(n+1)} + (\nabla g)^{(n+1)}(\theta - \theta^{(n+1)}) \\ &\quad + \tau(\theta - \theta^{(n+1)})^2, \end{aligned} \quad (59)$$

where  $g^{(n+1)}$  and  $(\nabla g)^{(n+1)}$  are updated as

$$g^{(n+1)} = (1 - \phi^{(n+1)})(g^{(n)}) + \phi^{(n+1)}T^{(n+1)} \quad (60)$$

$$(\nabla g)^{(n+1)} = (1 - \phi^{(n+1)})(\nabla g)^{(n)} + \phi^{(n+1)}(\nabla T)^{(n+1)}, \quad (61)$$

with  $g^{(0)} = 0$  and  $(\nabla g)^{(0)} = 0$ . Here,

$$(\nabla T)^{(n+1)} = \frac{a + b \log(1/\theta^{(n+1)}) - b(1/\theta^{(n+1)} - 1)}{(1 - \theta^{(n+1)})^2}, \quad (62)$$

where  $a = t_{d,B}^{(n+1)} + t_{d,W}^{(n+1)} + t_{u,W}^{(n+1)} + t_{u,B}^{(n+1)}$  and  $b = \nu \max_k \left( \frac{D_k c_k}{f_k} \right)$ . Since  $\tilde{g}^{(n+1)}(\theta)$  in (59) approximates  $g(\theta)$  in (37), problem (37) is finally approximated by the following convex problem:

**Algorithm 3** Training time minimization for FL on cell-free Massive MIMO networks

- 1: **Initialization:** Set  $n = 0$  and choose a random point  $\theta^{(n+1)} \in (0, 1)$ .
- 2: **repeat**
- 3:   A random  $\beta$  is realized for one large-scale coherence time
- 4:   Find the optimal solution  $(\boldsymbol{\eta}^*, \boldsymbol{\zeta}^*, \mathbf{f}^*, \mathbf{R}_d^*, \mathbf{R}_u^*)$  of the short-term subproblem (36) by using Algorithm 2
- 5:   Update  $(\boldsymbol{\eta}^{(n+1)}, \boldsymbol{\zeta}^{(n+1)}, \mathbf{f}^{(n+1)}, \mathbf{R}_d^{(n+1)}, \mathbf{R}_u^{(n+1)}) = (\boldsymbol{\eta}^*, \boldsymbol{\zeta}^*, \mathbf{f}^*, \mathbf{R}_d^*, \mathbf{R}_u^*)$
- 6:   Solve the approximate long-term master problem (63) to obtain its optimal solution  $\theta^*$
- 7:   Update  $\theta^{(n+2)}$  by (64)
- 8:   Update  $n = n + 1$
- 9: **until** convergence

**Output:**  $\theta^* = \theta^{(n+1)}$

$$\begin{aligned} \min_{\theta} \{ & g^{(n+1)} + (\nabla g)^{(n+1)}(\theta - \theta^{(n+1)}) + \tau(\theta - \theta^{(n+1)})^2 \} \\ \text{s.t. } & (35h). \end{aligned} \quad (63)$$

**C. Solving the Overall Problem (35)**

Algorithm 3 outlines the main steps to solve the overall problem (35). In the large-scale coherence time  $n$ , a random large-scale fading coefficient  $\beta$  is realized. For a given random value of  $\theta^{(n+1)} \in (0, 1)$ , one short-term subproblem (36) is solved by Algorithm 2 after  $I^{(n)}$  iterations to obtain a KKT solution. This solution is then used to construct the approximate long-term master problem (63). After solving (63) to obtain an optimal solution  $\theta^*$ , we update  $\theta^{(n+2)}$  as

$$\theta^{(n+2)} = (1 - \pi^{(n+1)})\theta^{(n+1)} + \pi^{(n+1)}\theta^*, \quad (64)$$

where  $\pi^{(n+1)}$  is a weighting parameter. Here,  $\{\phi^{(n)}, \pi^{(n)}\}$  is chosen to satisfy the following conditions [33, Assumption 5].

- (C1):  $\phi^{(n)} \rightarrow 0$ ,  $\frac{1}{\phi^{(n)}} \leq \mathcal{O}(n^\varsigma)$  for  $\varsigma \in (0, 1)$ , and  $\sum_n (\phi^{(n)})^2 < \infty$ ;
- (C2):  $\pi^{(n)} \rightarrow 0$ ,  $\sum_n \pi^{(n)} = \infty$ ,  $\sum_n (\pi^{(n)})^2 < \infty$ , and  $\lim_{n \rightarrow \infty} \frac{\pi^{(n)}}{\phi^{(n)}} = 0$ .

The REPEAT-UNTIL loop runs for  $N$  iterations before Algorithm 3 converges.

**D. The Proposed Algorithm: Implementation and Convergence Analysis**

Referring to Fig. 2 in Section III, Algorithm 3 is executed in the “FL performance optimization” interval. Specifically, Steps 3 and 4 takes place in the time block of STO, while steps 5 – 8 in the time block of LTO. Once Algorithm 3 converges, the FL process is then executed using the value of  $\theta$  given by Algorithm 3. Here, the performance of training update transmission in each iteration of the FL process is enhanced by updating  $(\boldsymbol{\eta}, \boldsymbol{\zeta}, \mathbf{f}, \mathbf{R}_d, \mathbf{R}_u)$  using Algorithm 2 in the STO time block. Whenever the statistics of large-scale fading changes, Algorithm 3 is executed again to make sure the FL performance is optimized with the updated statistics.

The convergence of Algorithm 3 is proved as follows. From the definitions of  $\tilde{z}_k(\varrho_k, R_{u,k})$ ,  $\tilde{h}_{d,k}(\mathbf{v})$ , and  $\tilde{h}_{u,k}(\mathbf{u})$  in (45),

(47) and (50), it can be verified that  $\tilde{z}_k(\varrho_k, R_{u,k})$ ,  $\tilde{h}_{d,k}(\mathbf{v})$  and  $\tilde{h}_{u,k}(\mathbf{u})$  have the following properties:

- $\tilde{z}_k(\varrho_k^{(n)}, R_{u,k}^{(n)}) = z_k(\varrho_k^{(n)}, R_{u,k}^{(n)})$ ,  $\tilde{h}_{d,k}(\mathbf{v}^{(n)}) = h_{d,k}(\mathbf{v}^{(n)})$ ,  $\tilde{h}_{u,k}(\mathbf{u}^{(n)}) = h_{u,k}(\mathbf{u}^{(n)})$ ,  $\nabla \tilde{z}_k(\varrho_k^{(n)}, R_{u,k}^{(n)}) = \nabla z_k(\varrho_k^{(n)}, R_{u,k}^{(n)})$ ,  $\nabla \tilde{h}_{d,k}(\mathbf{v}^{(n)}) = \nabla h_{d,k}(\mathbf{v}^{(n)})$ ,  $\nabla \tilde{h}_{u,k}(\mathbf{u}^{(n)}) = \nabla h_{u,k}(\mathbf{u}^{(n)})$ ;
- $\tilde{z}_k(\varrho_k, R_{u,k})$ ,  $-\tilde{h}_{d,k}(\mathbf{v})$ , and  $-\tilde{h}_{u,k}(\mathbf{u})$  are strongly convex;
- $\tilde{z}_k(\varrho_k, \varrho_k^{(n)}, R_{u,k}, R_{u,k}^{(n)})$  is Lipschitz continuous in all  $\varrho_k, \varrho_k^{(n)}, R_{u,k}, R_{u,k}^{(n)}$ ;  $\tilde{h}_{d,k}(\mathbf{v}, \mathbf{v}^{(n)})$  and  $\tilde{h}_{u,k}(\mathbf{u}, \mathbf{u}^{(n)})$  are Lipschitz continuous in both  $\mathbf{v}, \mathbf{v}^{(n)}$  and both  $\mathbf{u}, \mathbf{u}^{(n)}$ , respectively.

Algorithm 3 thus satisfies all the conditions for the short-term algorithm to work, as specified in the general framework [33, Assumption 2]. As such, the convergence of Algorithm 3 to a stationary point of problem (35) is guaranteed if  $I^{(n)} \rightarrow \infty$  and  $N \rightarrow \infty$  [33, Theorem 2]. In practice, since there are always numerical errors in computation, it is acceptable to choose finite  $\{I^{(n)}\}_{n \in \mathcal{N}}$  and  $N$ , where  $\mathcal{N} \triangleq \{1, \dots, N\}$ . Therefore, Algorithm 3 is then guaranteed to converge to the neighbourhood of the stationary solutions of problem (35) [33, Theorem 3].

## VII. CELL-FREE TDMA MASSIVE MIMO AND COLLOCATED MASSIVE MIMO FOR WIRELESS FEDERATED LEARNING

For comparison, this section introduces cell-free TDMA massive MIMO and collocated massive MIMO approaches that support wireless FL. Their associated problem formulations and solution algorithms are discussed in the following.

### A. Cell-Free TDMA Massive MIMO

The channel estimation of cell-free TDMA massive MIMO networks is equivalent to that of the cell-free massive MIMO networks where all the pilot are pairwisely orthogonal, i.e.,  $\varphi_\ell^H \varphi_k = 0, \forall \ell \in \mathcal{K} \setminus k$ . While cell-free TDMA massive MIMO networks only require the length of the pilot sequence  $\tilde{\tau}_t$  to be 1, cell-free massive MIMO networks require  $\tau_t \geq K$  for orthogonal pilots with  $K$  being the number of UEs.

In cell-free TDMA massive MIMO networks, the training update transmissions between the APs and  $K$  UEs happen in  $K$  equal orthogonal time slots. Therefore, a factor of  $(1/K)$  is imposed on the achievable DL and UL rates. Specifically, the achievable DL rate for a UE  $k$  is

$$R_{d,k} \leq \frac{\tau_c - \tilde{\tau}_t}{K\tau_c} B \log_2 \left( 1 + \frac{\rho_p \left( \sum_{m \in \mathcal{M}} \eta_{mk}^{1/2} \sigma_{mk}^2 \right)^2}{\rho_p \sum_{m \in \mathcal{M}} \eta_{mk} \sigma_{mk}^2 \beta_{mk} + 1} \right), \quad (65)$$

where  $\sigma_{mk}^2 = \frac{\tilde{\tau}_t \tilde{\rho}_t (\beta_{mk})^2}{\tilde{\tau}_t \tilde{\rho}_t \beta_{mk} + 1}$ , and  $\tilde{\rho}_t$  is the normalized signal-to-noise ratio (SNR) of each pilot symbol. The achievable UL rate  $R_{u,k}$  for a UE  $k$  is

$$R_{u,k} \leq \frac{\tau_c - \tilde{\tau}_t}{K\tau_c} B \log_2 \left( 1 + \frac{\rho_u \zeta_k \left( \sum_{m \in \mathcal{M}} \sigma_{mk}^2 \right)^2}{\rho_u \zeta_k \sum_{m \in \mathcal{M}} \sigma_{mk}^2 \beta_{mk} + \sum_{m \in \mathcal{M}} \sigma_{mk}^2} \right). \quad (66)$$

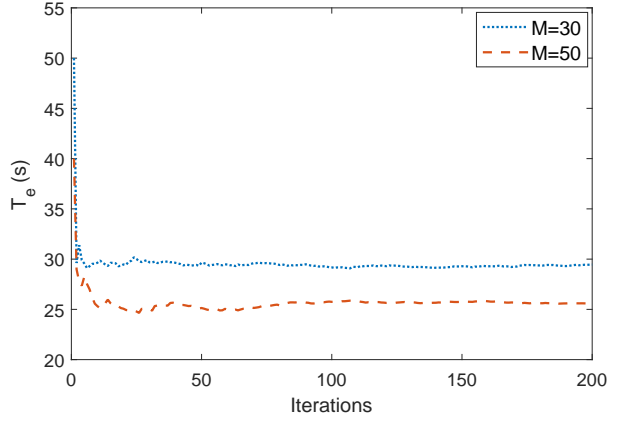


Fig. 4. The convergence of Algorithm 3. Here,  $K = 4$ .

Since the training updates are transmitted sequentially via wireless links, the effective training time of FL in cell-free TDMA massive MIMO networks is expressed as

$$\begin{aligned} & T_{\text{e,TDMA}}(\theta, \mathbf{f}, \mathbf{R}_d, \mathbf{R}_u) \\ & \triangleq G(\theta) \mathbb{E}\{T_{\text{G,TDMA}}(\theta, \mathbf{f}, \mathbf{R}_d, \mathbf{R}_u)\} \\ & \triangleq \vartheta \log \left( \frac{1}{\epsilon} \right) \mathbb{E} \left\{ \frac{1}{1-\theta} \left( t_{d,B}(\mathbf{R}_d) + \sum_{k \in \mathcal{K}} t_{d,k}(R_{d,k}) \right. \right. \\ & \quad \left. \left. + \max_{k \in \mathcal{K}} t_{C,k}(\theta, f_k) + \sum_{k \in \mathcal{K}} t_{u,k}(R_{u,k}) + t_{u,B}(\mathbf{R}_u) \right) \right\} \\ & \triangleq \vartheta \log \left( \frac{1}{\epsilon} \right) \mathbb{E}\{T_{\text{TDMA}}(\theta, \mathbf{f}, \mathbf{R}_d, \mathbf{R}_u)\}. \end{aligned} \quad (67)$$

The problem of FL training time minimization for cell-free TDMA massive MIMO is formulated as:

$$\min_{\boldsymbol{\eta}, \boldsymbol{\zeta}, \theta, \mathbf{f}, \mathbf{R}_d, \mathbf{R}_u} \mathbb{E}\{T_{\text{TDMA}}(\theta, \mathbf{f}, \mathbf{R}_d, \mathbf{R}_u)\} \quad (68a)$$

$$\text{s.t. (21), (35b) -- (35h), (65), (66)} \\ \sigma_{mk}^2 \eta_{mk} \leq 1, \forall m. \quad (68b)$$

Since problem (68) has the same mathematical structure as (35), the former can be solved by a slightly modified version of Algorithm 3 proposed in Section VI.

### B. Collocated Massive MIMO

A collocated massive MIMO network is a special case of a cell-free massive MIMO network where all the APs are collocated. Therefore,  $\beta_{mk} = \beta_k$  and  $\sigma_{mk}^2 = \sigma_k^2, \forall k \in \mathcal{K}$ . The DL power control coefficient  $\eta_k, \forall k \in \mathcal{K}$ , is constrained by

$$\sum_{k \in \mathcal{K}} \sigma_k^2 \frac{\eta_k}{M} \leq 1. \quad (69)$$

From (18) and (26), the achievable DL and UL rates for UE  $k$  are respectively designed as (70) and (71) [see the top of next page]. The problem of FL training time minimization for collocated massive MIMO is formulated as:

$$\min_{\boldsymbol{\eta}, \boldsymbol{\zeta}, \theta, \mathbf{f}, \mathbf{R}_d, \mathbf{R}_u} \mathbb{E}\{T(\theta, \mathbf{f}, \mathbf{R}_d, \mathbf{R}_u)\} \quad (72)$$

$$\text{s.t. (21), (35b) -- (35h), (69) -- (71).}$$

Similar to (68), problem (72) can be solved by a slightly modified version of Algorithm 3 in Section VI.

$$R_{d,k} \leq \frac{\tau_c - \tau_t}{\tau_c} B \log_2 \left( 1 + \frac{\rho_p M \eta_k \sigma_k^4}{\rho_p \sum_{\ell \in \mathcal{K} \setminus k} M \eta_\ell \left( \sigma_\ell^2 \frac{\beta_k}{\beta_\ell} \right)^2 |\boldsymbol{\varphi}_\ell^H \boldsymbol{\varphi}_k|^2 + \rho_p \sum_{\ell \in \mathcal{K}} \eta_\ell \sigma_\ell^2 \beta_k + 1} \right) \quad (70)$$

$$R_{u,k} \leq \frac{\tau_c - \tau_t}{\tau_c} B \log_2 \left( 1 + \frac{\rho_u M \zeta_k \sigma_k^2}{\rho_u \sum_{\ell \in \mathcal{K} \setminus k} \zeta_\ell M \sigma_k^2 \left( \frac{\beta_\ell}{\beta_k} \right)^2 |\boldsymbol{\varphi}_k^H \boldsymbol{\varphi}_\ell|^2 + \rho_u \sum_{\ell \in \mathcal{K}} \zeta_\ell \beta_\ell + 1} \right). \quad (71)$$

### VIII. NUMERICAL EXAMPLES

#### A. Parameters and Setup

We consider a cell-free massive MIMO network with  $\tau_c = 200$  samples. The APs and UEs are located in a square of  $D \times D$  km<sup>2</sup> whose edges are wrapped around to avoid the boundary effects. The large-scale fading coefficients, e.g.,  $\beta_{mk}$ , are modeled in the same manner as [48]

$$\beta_{mk} = 10^{\frac{\text{PL}_{mk}^d}{10}} 10^{\frac{\sigma_{shd}^d}{10} \frac{d_{mk}}{10}}, \quad (73)$$

where  $10^{\frac{\sigma_{shd}^d}{10} \frac{d_{mk}}{10}}$  represents the log-normal shadowing with the standard deviation  $\sigma_{shd}$  (in dB); and  $10^{\frac{\text{PL}_{mk}^d}{10}}$  represents the three-slope path loss.  $\text{PL}_{mk}^d$  (in dB) is given by

$$\text{PL}_{mk}^d = \begin{cases} -L - 35 \log_{10}(d_{mk}), & \text{if } d_{mk} > d_1, \\ -L - 15 \log_{10}(d_1) - 20 \log_{10}(d_{mk}), & \text{if } d_0 < d_{mk} \leq d_1, \\ -L - 15 \log_{10}(d_1) - 20 \log_{10}(d_0), & \text{if } d_{mk} \leq d_0, \end{cases} \quad (74)$$

where  $L$  is a constant depending on the carrier frequency, the UE and AP heights. For channel estimation, a scheme of random pilot is used in the time block of UL training. Specifically, the pilot of each user is randomly chosen from a predefined set of  $\tau_t$  orthogonal pilot sequences of length  $\tau_t$  samples.

Here, we choose  $\sigma_{shd} = 8$  dB,  $d_0 = 10$  m,  $d_1 = 50$  m,  $L = 140.7$  dB, bandwidth  $B = 20$  MHz, noise figure  $F = 9$  dB [31],  $f_{k,\max} = f_{\max} = 3.0 \times 10^9$  cycles/s,  $f_{k,\min} = f_{\min} = 1 \times 10^6$  cycles/s,  $D_k = \hat{D} = 7.5$  MB,  $c_k = c = 20$  cycles/sample,  $\forall k$ ,  $\nu = \vartheta = 1$ ,  $S_d = S_u = 4.5$  KB,  $\alpha = 2 \times 10^{-28}$  [18],  $E_{k,\max} = E_{\max} = 15$  J,  $\theta_{\max} = -10$  dB,  $\theta_{\min} = -60$  dB, and  $\epsilon = \varepsilon = 10^{-2}$ . Noise power  $\sigma_0^2 = k_B T_0 B F = -92$  dBm, where  $k_B = 1.381 \times 10^{-23}$  Joules/K is the Boltzmann constant and  $T_0 = 290$  K is the noise temperature. Let  $\tilde{\rho}_d = 1$  W,  $\tilde{\rho}_u = 0.2$  W and  $\tilde{\rho}_t = 0.2$  W be the maximum transmit power of the APs, UEs and UL training pilot sequences, respectively. The maximum transmit powers  $\rho_d$ ,  $\rho_u$  and  $\rho_t$  are normalized by the noise power. We set  $\pi^{(n)} = \frac{1}{n}$  and  $\phi^{(n)} = \frac{1}{n^{7/8}}$  which satisfy conditions (C1) and (C2) in Section VI-C.

#### B. Results and Discussions

1) *Effectiveness of the proposed algorithm:* First, we evaluate the convergence behavior of the proposed Algorithm 3. Fig. 4 shows the effective training time  $T_e$  versus the number of iterations with  $D = 0.5$  km,  $K = 4$ ,  $\tau_t = 10$  and  $M = \{30, 50\}$  for an arbitrary large-scale fading realization. It can be seen from Fig. 4 that Algorithm 3 converges in fewer than 100 iterations. It is also worth noting that each iteration of Algorithm 3 corresponds to solving simple convex programs

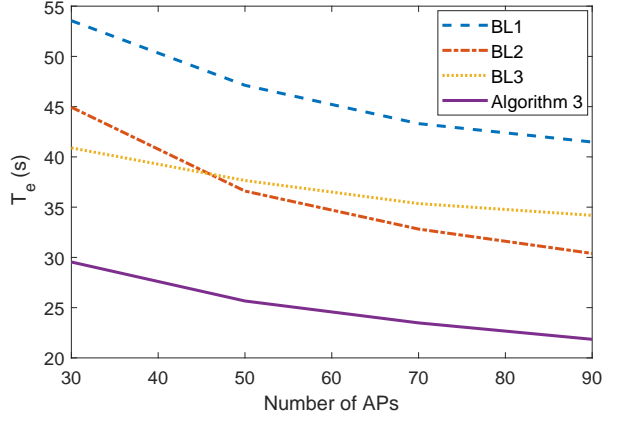


Fig. 5. Comparison among the baselines and Algorithm 3. Here,  $K = 4$ .

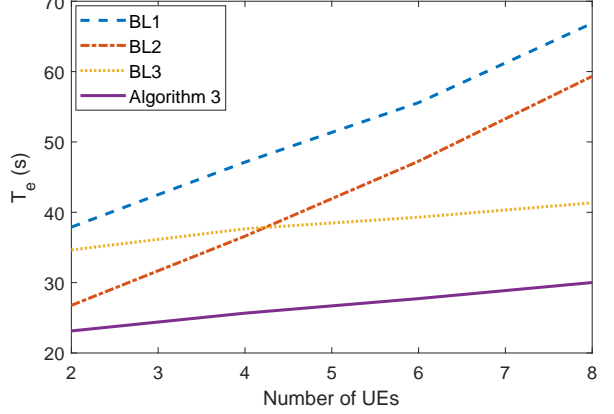


Fig. 6. Comparison among the baselines and Algorithm 3. Here,  $M = 50$ .

(55) and (63). It is therefore expected that Algorithm 3 has a low computational complexity.

To further evaluate the effectiveness of Algorithm 3, we consider the following baseline schemes:

- Baseline 1 (BL1): The DL powers allocated to all UEs are the same, i.e.,  $\eta_{mk} \sigma_{mk}^2 = 1/K, \forall m, k$ . The transmitted UL power of each UE is maximum, i.e.,  $\zeta_k = 1, \forall k$ . The local accuracy is fixed, i.e.,  $\theta = \frac{\theta_{\max} + \theta_{\min}}{2}$  dB. The data rates and processing frequencies of UEs are then optimized.
- Baseline 2 (BL2): This baseline is similar to BL1 except that  $\theta$  is optimized by a slightly modified version of Algorithm 3 (without using Algorithm 2).
- Baseline 3 (BL3): This baseline is similar to BL1 except that the transmitted DL and UL powers are optimized

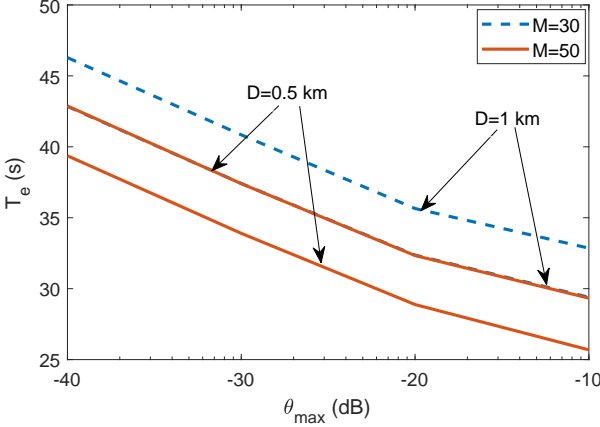


Fig. 7. Impact of the local accuracy on the effective training time. Here,  $K = 4$ .

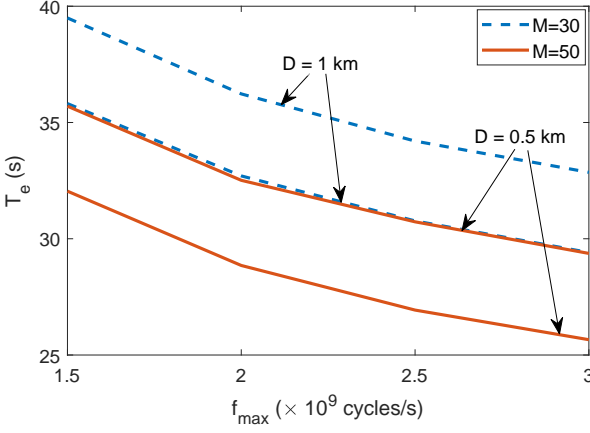


Fig. 8. Impact of UE's processing frequency on the effective training time. Here,  $K = 4$ .

by Algorithm 2. Here, the effective training time of FL is the averaged time of one FL process taken over the large-scale fading realizations.

Figs. 5 and 6 compare the effective training time  $T_e$  by the considered schemes. As seen, Algorithm 3 gives the best performance. In particular, compared to BL1, the time reduction by Algorithm 3 is up to 55% with  $M = 50$ ,  $K = 8$ . Note that BL2 and BL3 also perform much better than BL1, e.g., up to 29% in term of time reduction with  $M = 50$ ,  $K = 2$  and 38% with  $M = 50$ ,  $K = 8$ , respectively. Even so, Algorithm 3 still provides substantial time reductions over BL2 and BL3, e.g., up to 49% with  $M = 50$ ,  $K = 8$  and 43% with  $M = 90$ ,  $K = 4$ , respectively.

The figures not only show the importance of optimizing transmit power or local accuracy, but also demonstrate the noticeable advantage of joint optimization design. Moreover, thanks to the array gain, the data rates of UEs increase when the number of APs increases. This leads to the decrease in the effective training time as shown in Fig. 5. It can also be observed from Fig. 6 that a dramatic increase in the training time when the number of UEs increases. This is because the mutual interference and pilot contamination become stronger

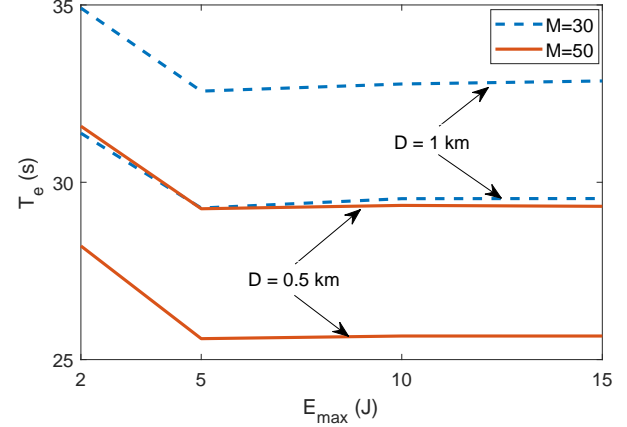


Fig. 9. Impact of UE's energy consumption limit  $E_{\max}$  on the effective training time. Here,  $K = 4$ .

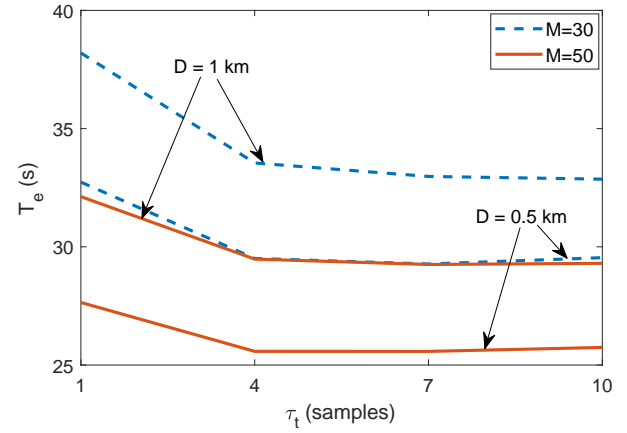


Fig. 10. Impact of the length of UL training pilots on the effective training time. Here,  $K = 4$ .

for a larger number of UEs.

2) *Impact of key system parameters on the effective training time:* The impact of the local accuracy on the effective training time is shown in Fig. 7. Decreasing the threshold  $\theta_{\max}$  leads to a dramatic increase in the effective training time, e.g., by up to 33% with  $\theta_{\max} = -40$  dB in comparison to that with  $\theta_{\max} = -10$ . This is reasonable because at a lower value of  $\theta$ , more iterations are required for local training. To keep the energy consumption of UEs below  $E_{\max}$ , the UEs' processing frequencies become smaller. This leads to an increase in the time required to compute the local training updates.

Fig. 8 shows the impact of UE's processing frequency on the effective training time. As seen, the effective training time increases when the threshold  $f_{\max}$  decreases. In particular, the increase is by up to 19% with  $f_{\max} = 1.5 \times 10^9$  cycles/s in comparison to that with  $f_{\max} = 3 \times 10^9$  cycles/s. This is because at a lower value of UEs' processing frequency, it requires more time to compute the local training updates.

In Fig. 9, the impact of UE's energy consumption limit  $E_{\max}$  on the effective training time is revealed. Here, decreasing  $E_{\max}$  leads to an increase in the effective time. Specifically, the increase is by up to 9.4% with  $E_{\max} = 2$

$J, D = 1$  km in comparison to that with  $E_{\max} = 15$  J,  $D = 1$  km. This is reasonable because at a low value of  $E_{\max}$ , the effective time may not approach the optimal value due to a smaller feasible region of the optimization problem (35).

Fig. 10 focuses on the impact of the length of UL training pilots on the effective training time. It is clear that too small and too large values of  $\tau_t$  both increase the effective time. Specially, the effective time increases up to 10% and 1% with  $\tau_t = 1$  and  $\tau_t = 13$  in comparison to that with  $\tau_t = 7$ , respectively. This is reasonable because at a large value of  $\tau_t$ , the factor of  $\frac{T_c - \tau_t}{T_c}$  makes the data rate decrease and the transmission time grows. In contrast, at a small value of  $\tau_t$ , the network suffers more from the pilot contamination, the data rates drop and the training update transmission time increases.

3) *Cell-free massive MIMO vs. Cell-free TDMA massive MIMO*: Fig. 11 compares the effective training time obtained from the cell-free TDMA massive MIMO with that from the cell-free massive MIMO where all the pilots are pairwisely orthogonal. For a fair comparison, we choose  $\tilde{\rho}_t = K\rho_t$  for the amount of energy consumed at the “UL training” time blocks of the two networks to be the same. We also choose  $\tau_t = K$  so that the powers of channel estimate, i.e.,  $\sigma_{mk}^2, \forall m, k$ , are the same in the two networks. From Fig. 11, a significant time reduction (e.g., of up to 94% with  $K = 8$ ) is achieved by the cell-free massive MIMO compared with the cell-free TDMA massive MIMO. This result is expected because in the former, the factor of  $(1/K)$  is imposed on the data rates and the training updates are transmitted sequentially. For a large number of UEs, the data rate is significantly small, and as a result, the training update transmission requires a substantially long time.

4) *Cell-free massive MIMO vs. Collocated massive MIMO*: Finally, we compare the effective training time in cell-free massive MIMO with that in collocated massive MIMO. Fig. 12 shows that the former significantly outperform the latter. E.g., the time reduction is by up to 33% with  $M = 30$  and  $D = 1$  km. The only case that latter outperforms the former is when the network coverage is small, e.g.,  $D = 0.5$  km. However, the gap in this case is under 1% and vanishes for  $M > 80$ . This observation is as expected because cell-free massive MIMO distributes antennas over their coverage area; and as such, their performance suffers less from the UEs with unfavorable links than that of collocated massive MIMO. Higher data rates and a lower training time then follow.

## IX. CONCLUSION

In this paper, we have proposed using cell-free massive MIMO networks to support FL in a wireless environment. We designed a general scheme in which any algorithm and beamforming/filtering approach can be further developed to optimize the performance of wireless FL. Specially here, each iteration of the FL optimization algorithms or the FL process happens only in one large-scale coherence time. Targeting training time minimization, we jointly design local accuracy, transmit power, data rate, and UE’s processing frequency under the practical requirements on the UE’s energy consumption limit and maximum transmit powers at the APs and UEs. A mixed timescale stochastic nonconvex optimization problem

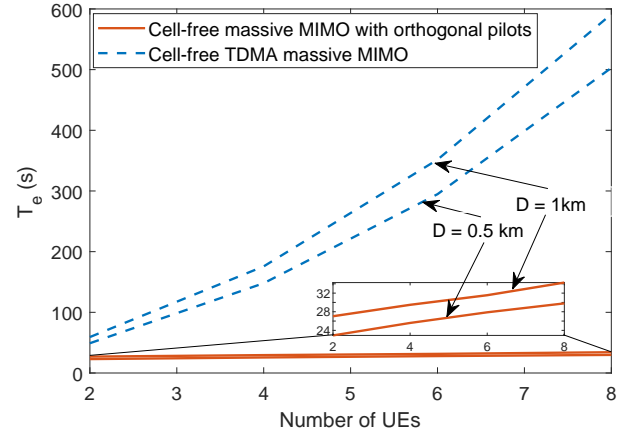


Fig. 11. Comparison between cell-free massive MIMO with orthogonal pilots and cell-free TDMA massive MIMO. Here,  $M = 50$ .

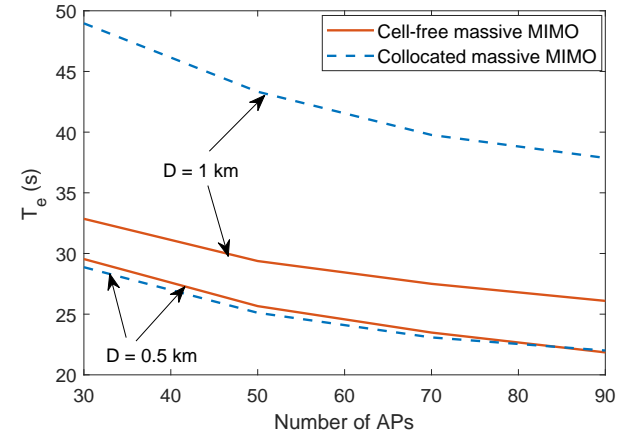


Fig. 12. Comparison between cell-free massive MIMO and collocated massive MIMO. Here,  $K = 4$ .

has been formulated with the objective of minimizing the training time of one FL process. Based on the general online successive convex approximation framework, we have developed a new algorithm to successfully solve the formulated problem. We have proved that the proposed algorithm converges to the neighborhood of stationary points of the optimization problem. For given parameter settings, numerical results show that our joint optimization design significantly reduces the training time of FL over the baselines under comparison. They have also confirmed that cell-free massive MIMO offers the lowest training time when compared with cell-free TDMA massive MIMO and collocated massive MIMO.

## REFERENCES

- [1] K. B. Letaief, W. Chen, Y. Shi, J. Zhang, and Y. A. Zhang, “The roadmap to 6G: AI empowered wireless networks,” *IEEE Commun. Mag.*, vol. 57, no. 8, pp. 84–90, Aug. 2019.
- [2] S. Dörner, S. Cammerer, J. Hoydis, and S. t. Brink, “Deep learning based communication over the air,” *IEEE J. Sel. Topics Signal Process.*, vol. 12, no. 1, pp. 132–143, Feb. 2018.
- [3] H. Sun, X. Chen, Q. Shi, M. Hong, X. Fu, and N. D. Sidiropoulos, “Learning to optimize: Training deep neural networks for interference management,” *IEEE Trans. Signal Process.*, vol. 66, no. 20, pp. 5438–5453, Oct. 2018.

[4] F. D. Calabrese, L. Wang, E. Ghadimi, G. Peters, L. Hanzo, and P. Soldati, "Learning radio resource management in RANs: Framework, opportunities, and challenges," *IEEE Commun. Mag.*, vol. 56, no. 9, pp. 138–145, Sep. 2018.

[5] J. Dong, M. Noreikis, Y. Xiao, and A. Yl-Jski, "Vinav: A vision-based indoor navigation system for smartphones," *IEEE Trans. Mobile Comput.*, vol. 18, no. 6, pp. 1461–1475, Jun. 2019.

[6] M. Zhou, Y. Tang, Z. Tian, L. Xie, and W. Nie, "Robust neighborhood graphing for semi-supervised indoor localization with light-loaded location fingerprinting," *IEEE Internet of Things J.*, vol. 5, no. 5, pp. 3378–3387, Oct. 2018.

[7] Y. LeCun, Y. Bengio, and G. Hinton, "Deep learning," *Nature*, vol. 521, no. 7553, pp. 436–444, May 2015.

[8] Qualcomm, "We are making on-device AI ubiquitous," <https://www.qualcomm.com/news/onq/2017/08/16/we-are-making-device-ai-ubiquitous>, 2017.

[9] Gartner, "Gartner highlights 10 uses for AI-powered smartphones," <https://www.gartner.com/en/newsroom/press-releases/2018-03-20-gartner-highlights-10-uses-for-ai-powered-smartphones>, 2018.

[10] G. Zhu, D. Liu, Y. Du, C. You, J. Zhang, and K. Huang, "Towards an intelligent edge: Wireless communication meets machine learning," 2018. [Online]. Available: <http://arxiv.org/abs/1809.00343>

[11] H. A. Alameddine, S. Sharafeddine, S. Sebbah, S. Ayoubi, and C. Assi, "Dynamic task offloading and scheduling for low-latency iot services in multi-access edge computing," *IEEE J. Sel. Areas Commun.*, vol. 37, no. 3, pp. 668–682, Mar. 2019.

[12] M. Chen and Y. Hao, "Task offloading for mobile edge computing in software defined ultra-dense network," *IEEE J. Sel. Areas Commun.*, vol. 36, no. 3, pp. 587–597, Mar. 2018.

[13] T. X. Tran, A. Hajisami, P. Pandey, and D. Pompili, "Collaborative mobile edge computing in 5G networks: New paradigms, scenarios, and challenges," *IEEE Commun. Mag.*, vol. 55, no. 4, pp. 54–61, Apr. 2017.

[14] C. Ma, J. Li, M. Ding, H. H. Yang, F. Shu, T. Q. S. Quek, and H. V. Poor, "On safeguarding privacy and security in the framework of federated learning," 2019. [Online]. Available: <https://arxiv.org/abs/1909.06512>

[15] T. Li, A. K. Sahu, A. Talwalkar, and V. Smith, "Federated learning: Challenges, methods, and future directions," 2019. [Online]. Available: <https://arxiv.org/abs/1908.07873>

[16] B. McMahan, E. Moore, D. Ramage, S. Hampson, and B. A. y Arcas, "Communication-efficient learning of deep networks from decentralized data," in *Proc. Int. Conf. Artificial Intell. Stat. (AISTATS)*, 2017, pp. 1273–1282.

[17] J. Konečný, H. B. McMahan, D. Ramage, and P. Richtárik, "Federated optimization: Distributed machine learning for on-device intelligence," 2016. [Online]. Available: <https://arxiv.org/abs/1610.02527>

[18] N. H. Tran, W. Bao, A. Zomaya, N. Minh N.H., and C. S. Hong, "Federated learning over wireless networks: Optimization model design and analysis," in *Proc. IEEE Conf. Comput. Commun. (INFOCOM)*, Apr. 2019, pp. 1387–1395.

[19] A. Hard, K. Rao, R. Mathews, F. Beaufays, S. Augenstein, H. Eichner, C. Kiddon, and D. Ramage, "Federated learning for mobile keyboard prediction," 2018. [Online]. Available: <http://arxiv.org/abs/1811.03604>

[20] K. Bonawitz, H. Eichner, W. Grieskamp, D. Huba, A. Ingeman, V. Ivanov, C. Kiddon, J. Konečný, S. Mazzocchi, H. B. McMahan, T. V. Overeldt, D. Petrou, D. Ramage, and J. Roslander, "Towards federated learning at scale: System design," 2019. [Online]. Available: <http://arxiv.org/abs/1902.01046>

[21] F. Sattler, S. Wiedemann, K. Müller, and W. Samek, "Robust and communication-efficient federated learning from Non-IID data," 2019. [Online]. Available: <http://arxiv.org/abs/1903.02891>

[22] A. K. Sahu, T. Li, M. Sanjabi, M. Zaheer, A. Talwalkar, and V. Smith, "On the convergence of federated optimization in heterogeneous networks," 2018. [Online]. Available: <http://arxiv.org/abs/1812.06127>

[23] J. Kang, Z. Xiong, D. Niyato, H. Yu, Y. Liang, and D. I. Kim, "Incentive design for efficient federated learning in mobile networks: A contract theory approach," 2019. [Online]. Available: <http://arxiv.org/abs/1905.07479>

[24] S. Wang, T. Tuor, T. Salonidis, K. K. Leung, C. Makaya, T. He, and K. Chan, "Adaptive federated learning in resource constrained edge computing systems," *IEEE J. Sel. Areas Commun.*, vol. 37, no. 6, pp. 1205–1221, Jun. 2019.

[25] K. Yang, T. Jiang, Y. Shi, and Z. Ding, "Federated learning via over-the-air computation," 2018. [Online]. Available: <http://arxiv.org/abs/1812.11750>

[26] Q. Zeng, Y. Du, K. K. Leung, and K. Huang, "Energy-efficient radio resource allocation for federated edge learning," 2019. [Online]. Available: <http://arxiv.org/abs/1907.06040>

[27] M. Chen, Z. Yang, W. Saad, H. V. Poor, and S. Cui, "A joint learning and communications framework for federated learning over wireless networks," 2019. [Online]. Available: <https://arxiv.org/abs/1909.07972>

[28] J. Zhang, S. Chen, Y. Lin, J. Zheng, B. Ai, and L. Hanzo, "Cell-free massive MIMO: A new next-generation paradigm," *IEEE Access*, vol. 7, pp. 99 878–99 888, 2019.

[29] M. Bashar, K. Cumanan, A. G. Burr, H. Q. Ngo, E. G. Larsson, and P. Xiao, "Energy efficiency of the cell-free massive MIMO uplink with optimal uniform quantization," *IEEE Trans. Green Commun. Netw.*, pp. 1–1, 2019.

[30] M. Bashar, K. Cumanan, A. G. Burr, M. Debbah, and H. Q. Ngo, "On the uplink maxmin SINR of cell-free massive MIMO systems," *IEEE Trans. Wireless Commun.*, vol. 18, no. 4, pp. 2021–2036, Apr. 2019.

[31] H. Q. Ngo, A. Ashikhmin, H. Yang, E. G. Larsson, and T. L. Marzetta, "Cell-free massive MIMO versus small cells," *IEEE Trans. Wireless Commun.*, vol. 16, no. 3, pp. 1834–1850, Mar. 2017.

[32] T. L. Marzetta, E. G. Larsson, H. Yang, and H. Q. Ngo, *Fundamentals of Massive MIMO*. Cambridge University Press, 2016.

[33] A. Liu, V. K. N. Lau, and M. Zhao, "Online successive convex approximation for two-stage stochastic nonconvex optimization," *IEEE Trans. Signal Process.*, vol. 66, no. 22, pp. 5941–5955, Nov. 2018.

[34] C. Ma, J. Konečný, M. Jaggi, V. Smith, M. I. Jordan, P. Richtárik, and M. Takáč, "Distributed optimization with arbitrary local solvers," *Optimization Methods Software*, vol. 32, no. 4, pp. 813–848, Jul. 2017.

[35] J. Ahn, O. Simeone, and J. Kang, "Wireless federated distillation for distributed edge learning with heterogeneous data," 2019. [Online]. Available: <http://arxiv.org/abs/1907.02745>

[36] M. Mohri, G. Sivek, and A. T. Suresh, "Agnostic federated learning," 2019. [Online]. Available: <http://arxiv.org/abs/1902.00146>

[37] H. Zhu and Y. Jin, "Multi-objective evolutionary federated learning," 2018. [Online]. Available: <http://arxiv.org/abs/1812.07478>

[38] J. Konečný, Z. Qu, and P. Richtárik, "Semi-stochastic coordinate descent," *Optimization Methods and Software*, vol. 32, no. 5, pp. 993–1005, 2017.

[39] M. Jaggi, V. Smith, M. Takáč, J. Terhorst, S. Krishnan, T. Hofmann, and M. I. Jordan, "Communication-efficient distributed dual coordinate ascent," in *Proc. 27th Int. Conf. Neural Inform. Process. Syst. (NIPS)*, vol. 2, 2014, pp. 3068–3076.

[40] S. M. Kay, *Fundamentals of Statistical Signal Processing: Estimation Theory*. Upper Saddle River, NJ, USA: Prentice-Hall, Inc., 1993.

[41] E. Björnson, J. Hoydis, and L. Sanguinetti, "Massive MIMO networks: Spectral, energy, and hardware efficiency," *Found. Trends. Signal Process.*, vol. 11, no. 3–4, pp. 154–655, 2017.

[42] A. P. Miettinen and J. K. Nurminen, "Energy efficiency of mobile clients in cloud computing," in *Proc. 2nd USENIX Conf. HotCloud*, 2010.

[43] S. Boyd and L. Vandenberghe, *Convex Optimization*. New York, NY: Cambridge University Press, 2004.

[44] T. T. Vu, D. T. Ngo, M. N. Dao, S. Durrani, D. H. N. Nguyen, and R. H. Middleton, "Energy efficiency maximization for downlink cloud radio access networks with data sharing and data compression," *IEEE Trans. Wireless Commun.*, vol. 17, no. 8, pp. 4955–4970, Aug. 2018.

[45] V. D. Nguyen, T. Q. Duong, H. D. Tuan, O. S. Shin, and H. V. Poor, "Spectral and energy efficiencies in full-duplex wireless information and power transfer," *IEEE Trans. Commun.*, vol. 65, no. 5, pp. 2220–2233, May 2017.

[46] V.-D. Nguyen, H. V. Nguyen, C. T. Nguyen, and O. Shin, "Spectral efficiency of full-duplex multi-user system: Beamforming design, user grouping, and time allocation," *IEEE Access*, vol. 5, pp. 5785–5797, 2017.

[47] B. R. Marks and G. P. Wright, "A general inner approximation algorithm for nonconvex mathematical programs," *Operations Research*, vol. 26, no. 4, pp. 681–683, 1978.

[48] H. Q. Ngo, L. Tran, T. Q. Duong, M. Matthaiou, and E. G. Larsson, "On the total energy efficiency of cell-free massive MIMO," *IEEE Trans. Green Commun. Netw.*, vol. 2, no. 1, pp. 25–39, Mar. 2018.